CHALMERS

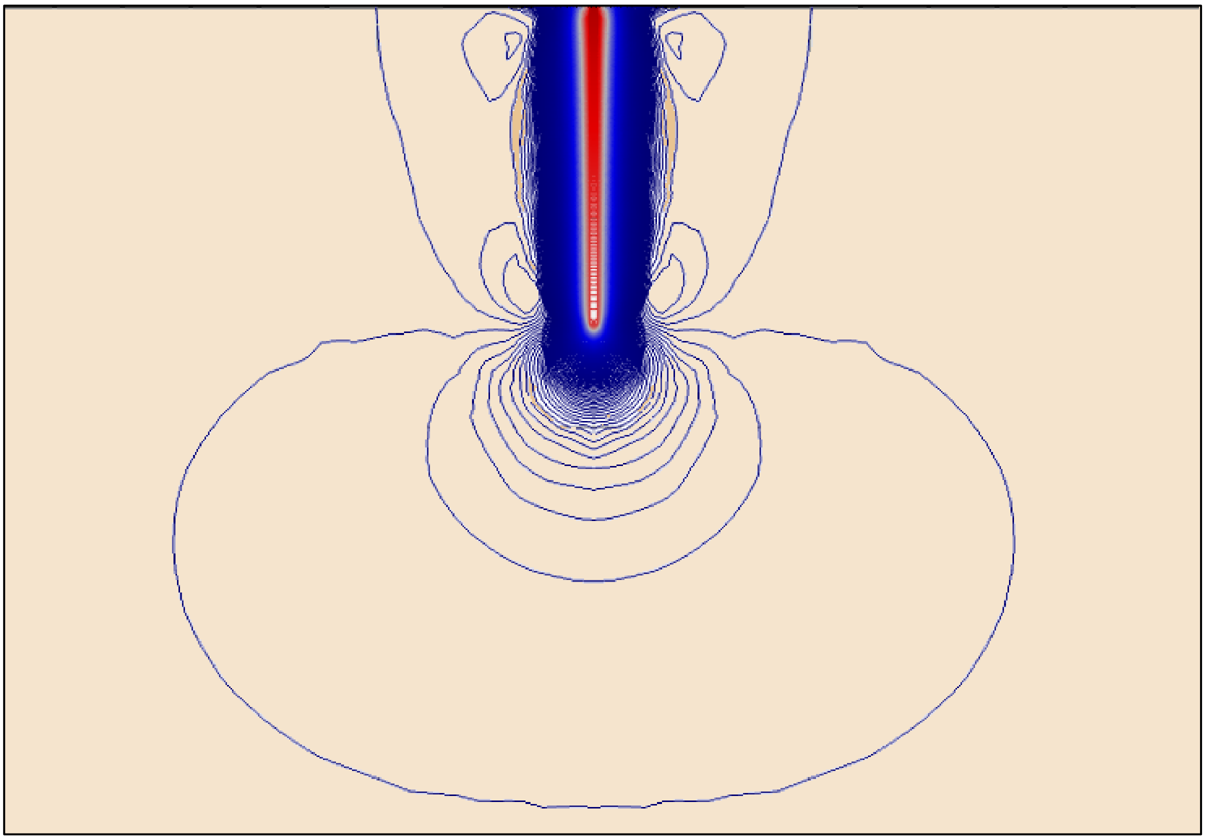

A Dynamic Response Study on Optimal Piling Depth with respect to Ground Vibrations

Master's Thesis in the Master's programme in Sound and Vibration

ERIK OLSSON

Department of Civil and Environmental Engineering
Division of Applied Acoustics
Vibroacoustics Group
CHALMERS UNIVERSITY OF TECHNOLOGY
Göteborg, Sweden 2014
Master's Thesis 2014:5

MASTER'S THESIS 2014:5

A Dynamic Response Study on Optimal Piling Depth with respect to Ground Vibrations

ERIK OLSSON

Department of Civil and Environmental Engineering
Division of Applied Acoustics
Vibroacoustics Group
CHALMERS UNIVERSITY OF TECHNOLOGY
Göteborg, Sweden 2014

A Dynamic Response Study on Optimal Piling Depth with respect to Ground Vibrations

Master's Thesis 2014:5

Department of Civil and Environmental Engineering
Division of Applied Acoustics
Vibroacoustics Group
Chalmers University of Technology
SE-41296 Göteborg
Sweden

Tel. +46-(0)31 772 1000

Reproservice / Department of Civil and Environmental Engineering
Göteborg, Sweden 2014

A Dynamic Response Study on Optimal Piling Depth with respect to Ground Vibrations
Master's Thesis in the Master's program in Sound and Vibration
Erik Olsson
Department of Civil and Environmental Engineering
Division of Applied Acoustics
Vibroacoustics Group
Chalmers University of Technology

Abstract

Dynamic response of a piled foundation in soil has lately received much attention in research areas such as civil engineering and seismic engineering. The goal of this thesis is to learn more about the dynamic response of a single pile in clay and in particular to study if there is an optimal piling depth. The clay types investigated are an idealized isotropic clay and a case-specific for *Gamla Ullevi*, Gothenburg, Sweden. The motion and forces are small and the soils are considered as linear elastic materials.

A solid finite element model is built in one case-specific and one idealized version. The idealized version is validated by mechanical response theory of a elastic half-space and also by comparison to a semi-analytical wavenumber model published 2013 by Kuo & Hunt. The response results show perfect agreement with half-space response theory and good agreement with the wavenumber model.

The point mobility of a vertically loaded pile, and the transfer mobility at surface and in depth, are studied for different pile lengths for frequencies below 20 Hz. The results from both finite element model and the wavenumber model show convergence piling depth at about 30 meters for both soil types. The transfer function results are reciprocal which allows to consider the foundation as the recipient of ground vibrations.

Keywords: Pile-soil dynamics, Mobility, Ground vibrations

Contents

Acknowledgements

Thank You Gunnar Widén at Akustikon/Norconsult for initiating this project and giving me the opportunity to work on it. Huge thanx for excellent supervision and explanations! Also thanks to Lisa and Andreas at Akustikon/Norconsult for letting me participate in our work.

My deepest gratitude goes to Associate professor Patrik Andersson at Applied Acoustics, Chalmers University for being my every-day supervisor, giving wise answers on stupid questions, spending hours of private time troubleshooting my Matlab-code.

Thank You to Daniel Ericsson at Comsol AB for giving excellent service and commitment in my project.

Thanks Börje Wiik and Gunilla Skog at Applied Acoustics for priceless help.

Thank You colleagues, class-mates and friends at Applied Acoustics, Chalmers University. Especially Amr and Erik whom I mostly shared the everyday progress and setbacks with during our thesis work.

Love and Joy to Märta and Ivar for giving and taking energy in a dynamic relationship. My wife to be, Anna, with patience out of this world, I Love You!

1. Introduction

1.1. Background

The environmental impact from noise and vibrations has gained increasing attention due to urbanization but also that people start to be more aware of the health issues.

Ground-borne vibrations is an acoustical science field linked to to geotechnics and seismology [Mol 00]. Ground vibrations are man-made, unlike seismology, were natural vibrations are studied. The transmission process from source to receiver is complex and depend on a number of factors. The vibrations are associated with different types of propagating elastic waves, i.e. surface waves or bulk waves.

1.2. Purpose and goal

The general purpose of this thesis is to learn more about ground vibrations and dynamic response of a pile foundation. This is achieved by a literature study consisting of research papers, educational books, information primers, standards and conversations with supervisors.

The specific goal is to find an optimal piling depth in clay with respect to ground vibrations. The goal is divided into two problem approaches:

- Optimal piling depth to minimize vibration radiation from a foundation.
- Optimal piling depth to anchor a receiver foundation against ground-borne vibrations from a distant source.

1.3. Limitations

The motions and forces involved are small and the responses are linear i.e. the soil is regarded as viscoelastic continuum (linear elastic media with time-dependent damping). The foundation is a single cylinder pile with constant surface area perfectly welded to the soil. The excitation and responses are in vertical direction. The frequency range of interest is typical for clay i.e. below 20 Hz.

1.4. Outline of thesis

In the next chapter some background to ground vibrations are mentioned; causes, effects, legislation and control actions. Background to soils, foundations and their interaction are briefly discussed and also a short research literature survey is included.

The third chapter comprises theory of an elastic half space concerning wave types and wave fields, dynamic response theory and a mobility approach is described and the models used in this theses; the finite element method (FEM) and a semianalytical wavenumber method by Kuo & Hunt (2013). Low strain condition is assumed meaning the soil behavior is linear.

Fourth chapter contains implementation procedures of a FEM models (one site-specific and one idealized) and the wavenumber model from literature for comparison. The single pile and soil FEM model is a symmetric quarter of a solid elastic half-space where the boundary conditions are full reflecting bedrock bottom, a free top surface and non-reflective background. The point mobilities at the top of the pile for different pile lengths in the frequency range below 20 Hz are examined. Different material properties are described.

Fifth chapter contains validation of the FEM model against dynamic response theory and comparison with the wavenumber model. The results of the response of the different models and for different material settings are presented.

The result and thesis is summarized and discussed in the last chapter.

2. Background to ground-borne vibrations

2.1. Causes, effects and control

2.1.1. Causes

Prominent sources of ground vibrations that is causing disturbance or building damage are construction work, blasting, vibrating machinery foundations or road or railway traffic.

Within construction activities impact pile driving is the most common source for noise and vibrations but vibratory driving of piles or sheets or vibratory compaction are other sources to ground vibration. Vibrations depend on the speed and the weight of the impact hammer which produces a shock wave in the pile creating shear waves at the pile lateral surface and pressure waves at the tip. The vibration magnitudes also depends on the ground conditions and the dynamic soil resistance. The pile radiates shear waves cylindrically and the tip radiates pressure waves spherically. The loading from the pile exceed the strength of the soil causing non-linear conditions.

Blasting in rock is regarded as a point source and the vibrations depending the detonating loading, clamping conditions and rock properties. Vibrations from blasting could be predicted by empirically relations [Mol 00].

Problems with traffic induced vibrations are mostly due to railway traffic because of its higher speeds and heavier loads. Prominent factors governing the vibrations from train traffic are; speed, load per axis, train length, unevenness of wheels, rail quality, and underground conditions. The frequency spectra of the induced vibrations depend on the speed, sleeper distance and the distance between wheel axis [Wid 13]. Long trains can be considered as a line source and within a distance of half the trains length there is no geometrical damping [Mol 00]. In clay soils the vibrations from heavy trains are in the frequency range below 10 Hz. Since freight trains normally are long the vibration period is long (5-40 seconds depending on length). In Sweden large infrastructure projects including underground railway tunnels are both planned and under construction and ground vibration issues are in question.

A rolling vehicle creates a depression in the ground due to its weight and energy is transferred into the ground. Critical is soft soils because the depression is larger creating larger dynamic response. Vibrations or shock caused by buses or heavy lorries passing over road humps is an example of environmental impact from road traffic.

Another cause of ground-borne vibrations of recent interest is crowd loads. An audience jumping up and down in phase can create considerable ground vibrations in soft soil grounds. Examples are the jumping football audience at *Gamla Ullevi* in Gothenburg, Sweden causing large vibrations in an adjacent multistory dwelling building. Another example from the same city is the rock concert audience at *Nya Ullevi* causing eigenmotion of the bearing pillars and wires of the arena [Erl 96].

2.1.2. Effects

Ground vibration considerations are gaining significance due to urbanization, use of more vibration sensitive equipment and peoples decreasing tolerance. The effect on humans is subjective and can vary from annoyance to illness. Determining factors could be; available previous information, age, worries about property, time of day and duration of vibration [Srb 10].

Traditionally railway noise has been regarded less annoying than road traffic and air plane noise. Recent studies shows that annoyance due to railway noise is increasing and that ground borne vibrations is one reason for that. Socio-acoustical field studies shows that the annoying noise level from railway traffic is 5-7 dB lower for people in areas subjected to ground-borne vibrations relative to areas without [Gid 12].

Damages on buildings is mostly cosmetic but can be cracking and fatigue. A heavy and stiff building is less effected than a light and soft building but in some cases a stiff building is more sensitive since it is less flexible. The rate of vibrations entering the building depends on the soil-foundation (and structure) interaction. At resonance with eigenfrequency of a building, structure or slab can amplification phenomena may occur [Srb 10].

Large ground vibrations can cause liquefaction i.e. the soil loosens its strength which in worst case can cause settlement, landslide etc. Luckily these occasions are rare in history.

2.1.3. Legislation

Activities where risk of unwanted vibration effects occur is regulated by standard norms. The norms in Sweden are:

1. SS 460 48 66 Vibrations from blasting
2. SS 02 52 11 Vibrations from demolition-, excavation-, pile driving- and compaction work
3. SS 460 48 61 Measurement methods of disturbance in dwellings and offices
4. SS 460 48 60 Inspection methods of building damages

1. and 2. contains method of calculating benchmark vibration levels to be used as vibration limits. The methods are based on relations between vertical peak particle velocity (PPV) measured on load bearing structure of the building and stated damage on the same building. Usually vibrations lower than 2 mm/s won't cause damages on buildings. If a building is damaged by ground vibrations the contractor is liable if benchmark values were exceeded. 1. and 2. do not consider sensitive equipment or psychological effects.

Norm 3. is based on international standard ISO 2631-2 which, in contrast to the SS-norm, differentiates continuous and transient vibrations and regards a number of factors that norm 3. does not [Hal 12]. ISO 2631-2 gives highest allowed vibrations of 0.4 mm/s (RMS) and 0.6 mm/s (PPV)($>$ 8Hz) in dwellings and offices. Norm 3. gives RMS-levels of vibrations for moderate disturbance (0.4-1.0 mm/s) and probable disturbance ($>$ 1.0 mm/s). These values are benchmark values which should be applied at new buildings. According to ISO2631 the human threshold on vibration sensitivity is 0.1-0.3 mm/s (RMS) in the frequency range 10 Hz to 100 Hz.
Swedish traffic authority *Trafikverket* has their own benchmark limits and values.

In norm 4 are methods for inspection and measurements of building described. A building subjected to vibration activity is inspected before, during and after the vibration activity. From a risk analysis assessment the most sensitive buildings are targeted for monitoring measurement (described in norm 3).

2.1.4. Prediction methods and control

Predicting ground vibrations and assessing legislation is a frequent engineering task [Srb 10]. Empirical methods based on known (i.e. measured) attenuation relationships are widely used but can be insufficient if there is a lack of source/path/receiver data. Numerical analysis can provide accurate predictions but require detailed ground properties, programming skills and computational time. Most reliable is small- or full scale testing which requires expertise, laboratory and/or equipment and is not frequently used. There are also a number of simplified case specific analysis (e.g. in [Srb 10]).

Vibration attenuation can be achieved preferable at the source, but also at the transmission path and/or at the receiver. By considerations of the foundation dynamics at the source, elastic bearings or dampers can be used, however rarely for frequencies below 8 Hz [Wid 13]. Control of structure-borne sound ($> 40Hz$ [Wid 13]) in underground train tunnels an be achieved by mounting the rails to elastic pads/mat. Example of active damping system at the source is the active control mass damper system at Gamla Ullevi attenuating crowd load induced vibrations.

At the the transmission path wave propagation barriers can be installed by absorbing or reflecting surface waves. Stiff barriers acts to average wave amplitudes over the barrier length and can be effective in the vertical direction, less effective in horizontal direction, since it is stiff in vertical direction [Srb 10]. Soft type barriers or trenches can prevent wave propagation but needs to be deep enough compared to the Rayleigh wave depth (see chapter 3). Another intervening technique is to install a row or multiple rows of thin shell-lined cylindrical holes [Ric 70]

Damping or isolation at the recipient might be needed if treatment at source or transmission path is unavailable. Example of such passive systems could be a type of foundation isolation against seismic activities.

2.2. Some words on piling and soils

2.2.1. Soils

Soil is the general term for the loose parts of the earth (i.e. not rock). The characteristics of the soil depends on the what materials it contains (e.g. mineral, grain size and water ratio) and the geometry arrangement (e.g. layering and texture).

Clay is a soil type with small weathered sheet-formed rock particles (grain size $<$ 0.002 mm [Sal 01]) which forms a fine structure. A clay sedimented in salty water has an open structure making it compressible. In the cavities (pores) there is chemically bounded water making the clay cohesive.

A soil can be consolidated at varying degrees. Consolidation depends on the stress history of the clay and normal consolidation means that a clay is today loaded by highest load experienced and over-consolidated means the clay is unloaded from earlier loading e.g. from glacial ice. Example of over-consolidated clay is the stiff sandy London clay. The clay in Gothenburg is normal-consolidated to slightly over-consolidated and highly saturated.

The strength and mechanical behavior of a soil is depending on the shear stiffness and the stress-strain relationship. The soil strength increases with depth due to the load from above lying soil layers. Ground water in the soil affects the soil strength and can be running free (e.g. through gravel or sand) or bounded chemically (e.g. around clay particles) or capillary (e.g. in pores [Sal 01]). Beneath the ground water level the effective stress from above lying layers is reduced due to hydrostatical pore pressure i.e. the water "lifts" the above layers.

The top soil layer closest to the surface is typically consisting of organic material, and clay drained from water, called dry crust.

2.2.2. Piling foundations

Piling foundations are used where soil conditions are insufficient to bear the static loading of a building, road or plant. The weight of the overlying structure is brought down to more solid ground (e.g. solid bedrock) making the pile end bearing.

Floating piles are used in cohesive soils where solid ground is unavailable. The static load on the pile is taken up by the cohesive forces around the surface area of the pile. The static load resistance in a floating pile is a function of the shear strength of the soil and the lateral surface area of the pile. The soil causes a horizontal soil pressure on the foundation which increases with depth. Sufficient piling depth depends not only on the load but also on the soil layers characteristics.

2.2.3. Pile-soil interaction

Foundations subjected to ground vibration can either attenuate or amplify the motion. In general, the interaction between ground vibration and foundation can be divided into kinematic interaction and inertial interaction. In kinematic interaction the foundation is unable to follow motion in the ground due to greater stiffness compared to the soil. Inertial interaction is caused by structural and foundation masses which follows the ground motion. When a motion period in the ground coincides with a period in the structure resonance occur which, of course, should be avoided [Srb 10].

2.3. Literature survey of pile dynamics

There is a wealth of information of dynamic response of pile foundations which mostly been studied by seismic and civil engineering. In the subsequent section a selection of methods and some findings throughout history is presented.

First to solve the problem of a harmonic surface load on a homogenous elastic half space was Lord Lamb 1904 [Lam 04] who also mathematically proved the surface wave found by Lord Rayleigh. Based on Lamb is [Ewi 57] where an interior point source (e.g. explosion) and wave propagation in a layered half space is discussed. In [Ric 70] interaction between soil and foundations are discussed primary directed towards machinery vibration.

Early studies of pile foundation response by was done by Novak. In [Nov 74] a method for determining dynamic stiffness and damping constants was derived by a semi-analytical elastic continuum approach. The soil enclosing the pile is regarded as a series of springs (a dynamic Winkler formulation) and the stiffness and damping of these springs are determined under plane-strain condition, meaning only horizontal wave propagation. The same approach is used in [Nov 77] where the motion of the pile tip is included and a soil layer beneath the pile (previous studies have been on end bearing piles). A floating pile was concluded having higher damping but lower stiffness than an end bearing pile.

In [Kay 91] the soil is an elastic continuum and displacement of a subsurface cylinder representing the pile is evaluated by integral transform techniques of the Greens functions in viscoelastic layered media.

Solutions for Greens function for layered media in wavenumber domain, together with boundary element method, for calculating wave propagation and soil-structure interaction for an interior source in a half space are used in i.e [Aue10].

Numerical methods such as boundary elements or finite elements are widely used e.g. [Wug 97]. Difficulties are the long computational times and since the underground often is very complex these models are generally reserved for final design stages.

An up-to-date contribution is [Kuo 13] where a novel single-pile model formulated in wavenumber domain and the soil regarded as viscoelastic continuum is presented. An axial loaded finite column is formulated using mirror image superposition of an infinite loading case. The pile head frequency response is treated and according to the authors the results show excellent agreement with existing models including a BEM-model but with with less computational time. Nor surface waves or depth dependent parameters are considered. However; It is mentioned that sufficient pile length for simulating infinite long pile in a full space is $40m - 50m$.

Influence of piling depth has been studied by [Nov 77] but also in [Ayo 12] where relations between the pile dimensions, the depth of fixity and the soil properties are measured through small scale measurements with a laterally loaded pile. An empirical relation depth of fixation and soil and pile properties is derived from multiple regression analysis.

These models all assume linear elastic conditions under small strains. Examples of non-linearity are high amplitudes or close to pile the soil could plasticize or rupture, slippage or gaps at pile-soil interface.

Described in a paper by Gladwell [Gla 68] the surface on a half space elastic solid is excited by a circular disc and an expression for the mechanical impedance is stated (based on results from Robertson [Rob 66]). Later Petersson [Pet 83] uses these results when simulating an elastic half space by a T-shaped body and states expression for the point mobility.

No numerical studies on driving point mobility of a axially loaded floating pile in soil with variable properties have been found.

3. Modelling pile dynamics and ground vibrations

3.1. Elastic half space

3.1.1. Wave types

The wave equation for motion in a homogenous isotropic elastic solid medium is

$$(\lambda + \mu)\frac{\partial \bar{\epsilon}}{\partial u} + \mu \nabla^2 u = \rho \frac{\partial^2 u}{\partial t^2} \tag{3.1}$$

in x direction where λ and μ are Lame's constants, ∇^2 is the Laplacian operator, u is the displacement, t is the time. It is written similarly in y and z directions with u changed to v and w respectively. $\bar{\epsilon}$ is the volume expansion defined as $\bar{\epsilon} = \epsilon_x + \epsilon_y + \epsilon_z$ i.e. the dilatation in all directions.

First solution for the equations of motion 3.1 is

$$\frac{\partial \bar{\epsilon}}{\partial t} = c_p^2 \nabla^2 \bar{\epsilon} \tag{3.2}$$

where

$$c_p = \sqrt{\frac{\lambda + 2G}{\rho}} \tag{3.3}$$

implying that volume expansion is propagating with speed c_p. In this P-wave (pressure wave, primary wave, compression wave, dilatational wave) the particle motion is in the same direction as the propagation.

The second solution to Eq. 3.1 is

$$\frac{\partial \bar{\omega}_x}{\partial t} = c_s^2 \nabla^2 \bar{\omega}_x \tag{3.4}$$

where $\bar{\omega}_x$ is the rotation about an axis (here x-axis, but similar expressions for y and z) and

$$c_s = \sqrt{\frac{G}{\rho}} \tag{3.5}$$

meaning that rotation is propagating with speed c_s. In the S-wave (shear waves, second waves, or transversal waves, distortional wave) the particle motion is perpendicular to the propagation direction and can be divided into two components; SV (motion in the vertical plane) and SH (motion in the horizontal plane) [Hal 12].

The traditional approach to ground dynamics is the use of an elastic, homogenous, isotropic half-space where a free surface is added and subjected to excitation and wave propagation. Interaction between P-wave, SV-wave and the shallow soil layer causes the Rayleigh wave, which is a third solution to the wave equation 3.1. The particle motion is elliptical and counterclockwise (propagating from left to right), a so called retrograde motion. The Rayleigh wave propagation speed is

$$c_r = c_s \frac{0.874 + 1.12\nu}{1 + \nu} \tag{3.6}$$

and the penetration depth depends roughly on the wavelength $\lambda = c_r/f$ [Hal 12]. The Rayleigh wave speed is slightly slower than the shear wave speed and considerably slower than the pressure wave speed, a relation depending on the Poissons number ν see figure 3.1(a). The Lowe surface wave is neglected here. The motion of the three prominent wave types on a elastic half space is showned in 3.1(b).

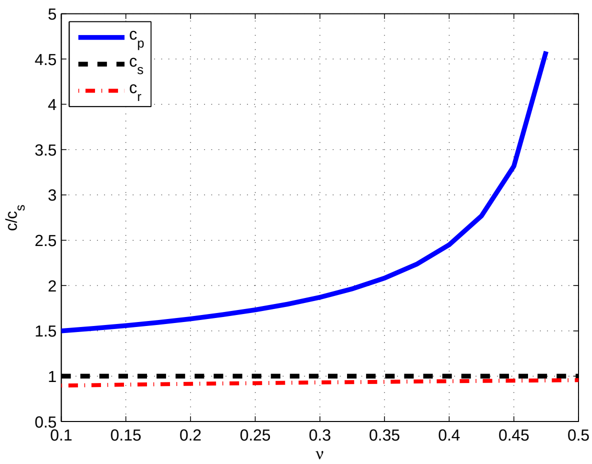

(a) Relative wavespeed

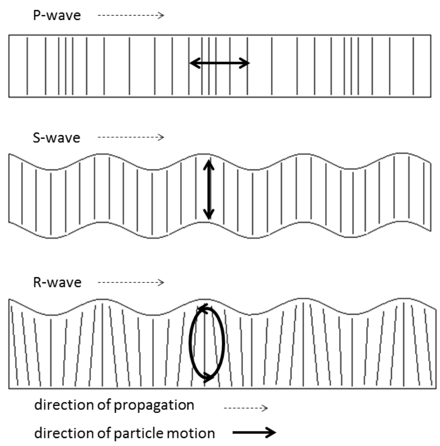

(b) Motions of prominent waves

Figure 3.1.: Characteristics for the prominent wave types (Taken from [Ric 70]). (a) x-axis: Relative wave speeds c/c_s [m/s] x-axis: Poissons number ν

The wave field generated by a circular footing is shown in figure 3.2. The bulk pressure wave and the bulk shear wave travel radially outwards and decays in the body, due to geometric damping, by r^{-1}. The bulk shear wave has a window of maximum displacement in about 45 degrees from the source. The surface pressure and shear waves decays by r^{-2}. The Rayleigh wave propagates cylindrically and decays by $r^{-0.5}$ for both components.

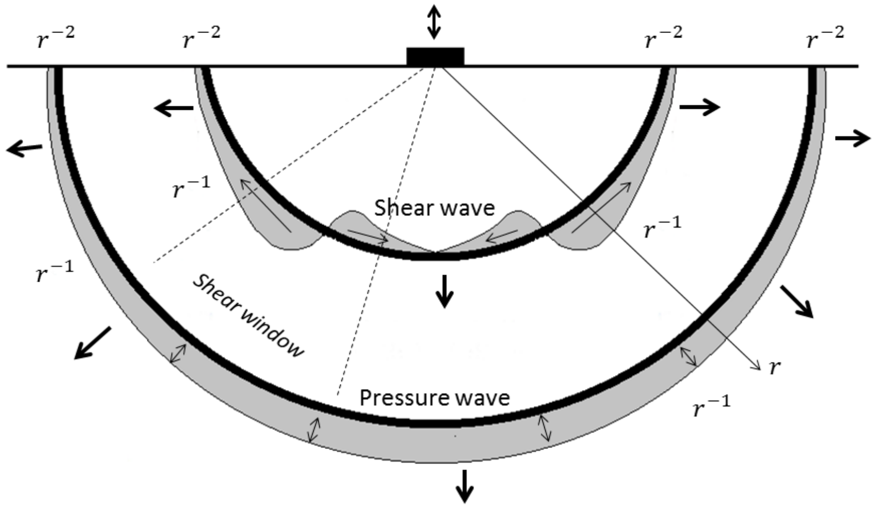

[Body wave field]

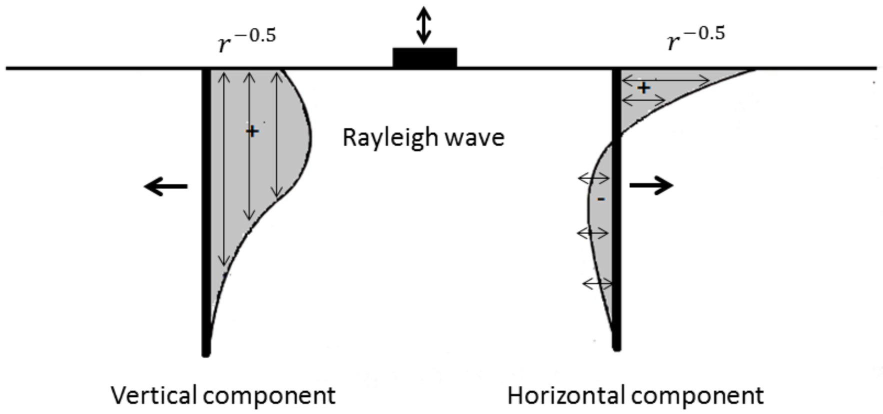

[Surface wave field]

Figure 3.2.: Wave field at a elastic halfspace excited at surface (based on Richart et. al 1970)

When a circular footing is excited at the surface as in figure 3.2, the energy is diverted in different wave types percent partition. For the example from literature: c_p : 7%,

c_s : 26% and c_r : 67% with poissons number $\nu = 0.25$. Thus the Rayleigh wave is the primary cause of structural movement on the surface or for shallow foundations [Ric 70].

3.1.2. Some wave phenomena

Some physical wave phenomena associated with ground vibrations are:

Refraction, reflection and diffraction
Huygens principle states that every point of a wave surface becomes in turn new sources of disturbance. It can be used for explaining propagation at reflecting surface and refraction around corners [Srb 10].

Frequency dispersion
In a homogenous soil the wave speed is constant with frequency but normally the stiffness of the soil is increasing with depth making the long Rayleigh wavelengths propagate at higher speed, a phenomenon called frequency dispersion. The phase wave speed and the group speed could be estimated from a phase-frequency plot. The speed of surface waves normally decrease with frequency.

Damping
The intensity of the wave energy propagating from a source decrease due to material damping and geometric damping [Hal 12]. Geometric damping depends on the wave front spreading over larger area decreasing its energy. The wave amplitude from a point excitation at the surface of a half space decreases as shown in section 3.1.1. Material damping is due to inner friction in the media of the propagating waves (the wave energy dissipates into heat). It can be divided into viscoelastic damping and hysteresis damping. In the viscous damping model the lost energy is independent of frequency and for the hysteresis damping model the lost energy is lost per cycle, frequency dependent.

The energy dissipation per cycle depends on the hysteresis damping

$$\xi = \frac{E_d}{4\pi E_s} = \frac{\eta}{2} \tag{3.7}$$

where ξ is the hysteresis damping ratio, E_d is the energy loss per cycle, E_s the maximal tension energy and η is the loss factor.

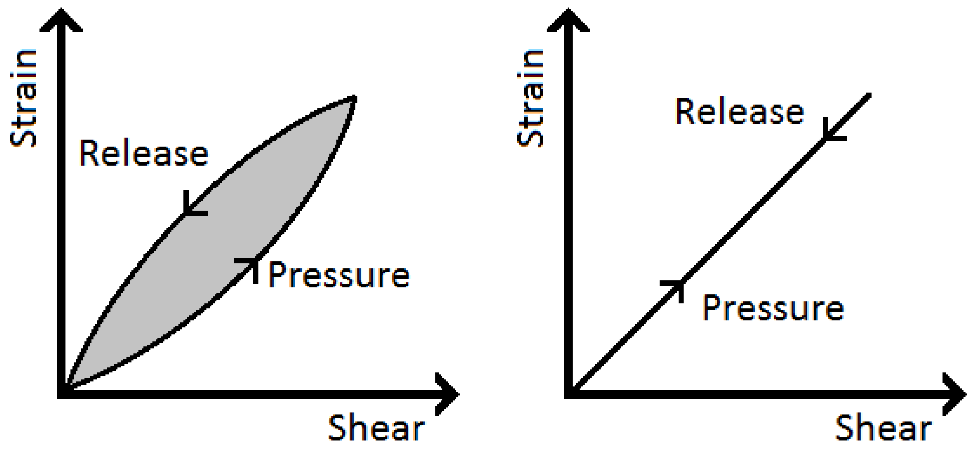

(a) Hysteresis (b) No damping

Figure 3.3.: Elastic models of dynamic motion. With (a) and without (b) viscous damping

Material damping is higher in lose soils than in stiffer soils resulting in that low frequency vibrations are spread to relatively large areas.

Radiation damping is coupled to a vibrating structure e.g. a pile in soil. The more damped the pile is, the more vibration is radiated into the soil. Radiation damping is further discussed in section 3.3.

3.2. Linear elastic model of soil

In the simplest form of stress-strain-time-model of a soil the material is elastic i.e. the stress and strain is linearly dependent and the dynamic properties are constant. The assumption of a linear elastic soil is valid for shear strains $\gamma_c < 10^{-4}$. For shear strains $10^{-}4 > \gamma_c < 10^{-2}$ the soil has elastoplastic behavior with permanent deformations (settlements and cracks). For shear strains $\gamma_c > 10^{-2}$ soil material could rupture (landslides and liquefaction). The governing material parameters for the soil behavior are the shear module G, poissons number ν and the material damping

The linear stress and strain relation is

$$\{\sigma\} = [D] \cdot \{\epsilon\} \tag{3.8}$$

where $[D]$ is the stiffness matrix and $\{\sigma\}$ and $\{\epsilon\}$ is the stress and strain vectors. An isotropic material has the same properties in all directions of $[D]$. A material with the same properties in one plane (e.g. the xy-plane) and and different properties in the normal direction to this plane (z-direction) is called transverse isotropic (which is a form of orthotropic). The elements in the different types of stiffness matrices $[D]$ are shown in appendix B together with stress and strain vectors $\{\sigma\}$ and $\{\epsilon\}$.

3.3. Mechanical response of a semi-infinite elastic space

Excitation of a structure by a force gives rise to a proportional motion (excluding extreme loads). The relation between the two interdependent quantities are called mechanical impedance Z or mechanical mobility Y which are complex ratios varying with frequency and reciprocals ($Y = Z^{-1}$). The definition for mobility is

$$\underline{\hat{Y}} = \frac{\underline{\hat{v}}}{\underline{\hat{F}}} \tag{3.9}$$

The underline indicates complex values and the hat peak values. Between the complex force and the complex velocity a phase relation exists which also is a function of frequency. The complex impedance could be written $Y = R + \imath X$ where $R = \Re\{Y\}$ is the resistive part and $X = \Im\{Y\}$ is the reactive part. In the resistive part the force and velocity are in phase representing energy transfer. In the reactive part the quantities are out of phase causing no energy transfer. The phase of the mobility $\angle Y$ is $\tan^{-1}(X/R)$ and the magnitude $|Y|$.

The response in the excitation point is called driving point mobility. Excitation in a point means that the excitation area is much smaller than the wavelength governing the propagation [Cre 05]. The response at another receiver point is called transfer mobility.

The conventional form for complex dynamic response of piles is in displacement impedance F/u [Kuo 13]. When discussing mobility, i.e. velocity response, the real part corresponds to pile axial dynamic damping and the imaginary part as the pile axial dynamic stiffness.

In the paper by Gladwell [Gla 68] an expression is stated (derived by Robertson [Rob 66]) for the mechanical impedance for an elastic half body excited perpendicular to the surface by an rigid indenter (small circular disk). Rigid means that the indenter is implying a uniform displacement over the indented area. The vertical displacement w due to an vertical force F is

$$\frac{w}{F} = \frac{1-\nu}{4Ga}(p_1 + \jmath * p_2) \tag{3.10}$$

where

$$p_1 = 1 - 0.198\beta^2 + 0.836\beta^4 \tag{3.11}$$

and

$$p_2 = 0.836\beta + 0.017\beta^3 \tag{3.12}$$

and $\beta = a\omega/c_s$ and a is the radius of the indenter. The values of the coefficients in equations 3.11 and 3.12 are valid for normal impedance for frictionless contact for $\nu = 0.5$ and$\beta < 0.7$ approximately [Gla 68].

The mechanical impedance of a damper is the damping constant c, the mechanical impedance of a spring is $-\jmath k/\omega$ and the combined (displacement) impedance is $Z = c + \frac{k}{\jmath\omega}$. The corresponding mobility can in these terms be expressed

$$Y = \frac{v}{F} = \frac{\jmath\omega}{k + \jmath\omega c} = \frac{\jmath\omega(k - \jmath\omega c)}{(k + \jmath\omega c)(k - \jmath\omega c)} = \frac{\omega^2 c}{k^2 + \omega^2 c^2} + \jmath\frac{\omega k}{k^2 + \omega^2 c^2} \tag{3.13}$$

In equation 3.13 it can be seen that the stiffness k is governing the response at low frequencies and the damping c at high frequencies. For low frequencies the imaginary part is increasing linearly with frequency (+6 dB per octave) and the real part is increasing with frequency squared (+12 dB per octave).

The power input into a structure is

$$W_{in} = \frac{1}{2} |F|^2 Re\{Y\} \tag{3.14}$$

meaning that the energy dissipated from a structure excited by constant force is solely depending on the real part of the mobility which depends on type of structure and excitation points on the structure.

3.4. Numerical modeling using finite elements

3.4.1. Basics of finite elements

The prominent numerical tool for solving partial differential equations (like the wave equation) is finite element method (FEM) due to its flexibility and generality [Num 06]. A very brief explanation follows:

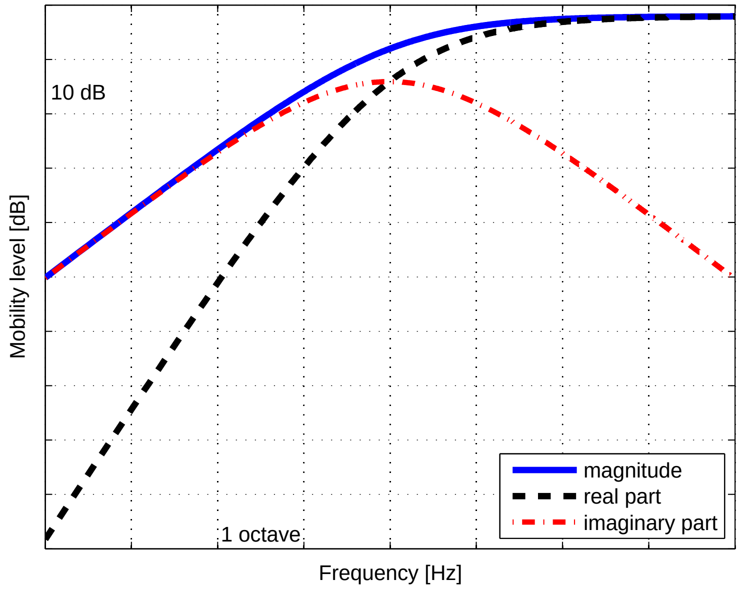

Figure 3.4.: The frequency dependence of the point mobility of an elastic half space

A problem domain is split into smaller sub-domains for which the solution is known, the sub problems are coupled together by known boundary conditions, leading to an equation system that has solutions at each couple point. The sub domains are called elements, the elements are made up by a grid of nodes, called a mesh. Inside an element, between the nodes, an interpolating shape function is used to assume a solution. The higher order on the shape function the more accurate solution.
The shape functions are used to assemble the system of equations into a system matrix representing e.g. a discrete system of masses connected by springs. Making the "right hand side" a vector of loads and boundary conditions is assembled, and the matrix system can be solved [Num 06].

An implementation of a mechanic continuum in a finite element software uses spatial coordinate system (x,y,z) and material coordinate system (X,Y,Z) which coincides when the displacement is zero [Com 12]. When deformed each material particle keeps its material coordinate system while the spatial coordinate system change with time t according to

$$\mathbf{x} = \mathbf{x}(\mathbf{X}, t) = \mathbf{X} + \mathbf{u}(\mathbf{X}, t) \tag{3.15}$$

where $\mathbf{u}$ is the displacement vector. The material coordinates relate to the original geometry and the spatial coordinates depends on the solution (i.e. displacement u).

The gradient of displacement, depending on material coordinates, for solid 3D in Lagrangian [1] formulation is

$$\nabla \mathbf{u} = \begin{bmatrix} \frac{\partial u}{\partial \mathbf{X}} & \frac{\partial u}{\partial \mathbf{Y}} & \frac{\partial u}{\partial \mathbf{Z}} \\ \frac{\partial v}{\partial \mathbf{X}} & \frac{\partial v}{\partial \mathbf{Y}} & \frac{\partial v}{\partial \mathbf{Z}} \\ \frac{\partial w}{\partial \mathbf{X}} & \frac{\partial w}{\partial \mathbf{Y}} & \frac{\partial w}{\partial \mathbf{Z}} \end{bmatrix} \tag{3.16}$$

The total strain tensor can then be expressed as

$$\epsilon = \frac{1}{2}(\nabla \mathbf{u} + \nabla \mathbf{u}^T) \tag{3.17}$$

The division by 2 of the shear modulus comes from the engineering shear strain approximation, saying that $\gamma_{xy} = \epsilon_{xy} + \epsilon_{yx} = 2\epsilon_{xy}$ corresponding to the total shear in a plane [Com 12].

3.4.2. Including damping in model

Hookes law (equation 3.8) is valid for elastic materials. When damping is included in the model the material becomes viscoelastic but elastic theory still holds for low damping and small force magnitudes [For 06]. When visco-elasticity is modeled in the frequency domain, material damping (or structural damping) is implemented as complex stiffness modulus E:

$$E = E' + \jmath E'' = E \cdot (1 + \jmath\eta) \tag{3.18}$$

where η is an isotropic loss factor ratio $\eta = E''/E'$ and E' storage module, defining the amount of stored energy in a cycle, E'' the loss modulus, defining the amount of energy dissipated as heat.

3.4.3. Infinite boundaries

A challenge in FEM modeling is how to create open boundaries in wave propagation. Infinite elements, impedance matching layers and perfectly matching domains are some methods to treat this problem.

[1] Lagrangian formulation means that generalized coordinates are used, referring to material configuration rather than any absolute coordinate system (e.g. Cartesian coordinates). The advantage is that spatially varying materials can be evaluated just once for the initial material configuration and do not change as the solid deforms [Com 12].

An impedance matching layer is a damper boundary condition where the damper has the same value as the wave impedance ρc. Since elastic bulk waves have different wave speeds a rough estimation of $Z = \frac{1}{2}\rho(c_p + c_s)$ is often used. [2]

A perfectly matching layer (PML) is an additional domain which functions as an absorber for incoming waves. In the FEM-software the PML is claimed to have good performance for a wide range of incident angles and not being sensitive to the shape of the wave front [Com 12]. It is implemented as a coordinate transform

$$t' = (\frac{t}{\Delta_w})^n \cdot (1 - \jmath) \cdot \lambda F \tag{3.19}$$

where t is the general coordinate variable, t′ the transformed PML coordinate, Δ_w is the thickness of the domain, n is the PML order, λ the typical wavelength of incident wave to be absorbed and F is a scaling factor. The PML is sensitive to complex shapes in the model and works best for simple geometries like squares, cylinders and spheres.

[2] In *Comsol Multiphysics* this impedance is the default for the *Low Reflecting Boundary* node. This function performs best for transient studies. An attempt to implement the impedance matching layer was made by using the *Spring Foundation* layer with each node in that layer having a specific damping in the three spatial components i.e. ρc_p in the normal direction to the layer and ρc_s in the both in-plane components. The result gave less reflections than the *Low Reflecting Boundary* function but the amount was not satisfactory low.

3.5. Wave number model for dynamic response

This model follows a paper by Kuo and Hunt published in 2013 [Kuo 13]. The semi-analytical model for dynamic behavior of piles is based on a so called pipe-in-pipe model used for underground railways [Cou 10]. The "inner pipe" is an infinite pile modeled as a column in axial vibration and the "outer pipe" is the soil modeled as a viscoelastic continuum with outer radius of infinity and inner radius equal to the radius of the pile.

The loading on the column from the surrounding medium consists of shear stress components which, in longitudinal direction (z-direction), is

$$\tau_{rz}(z,t) = \Re\left\{\tilde{T}_{rz}(\xi,\omega)\mathrm{e}^{\jmath\xi z}\mathrm{e}^{\jmath\omega t}\right\} \tag{3.20}$$

and the displacement of the continuum is in a similar expression

$$u_z(z,t) = \Re\left\{\tilde{U}_z(\xi,\omega)\mathrm{e}^{\jmath\xi z}\mathrm{e}^{\jmath\omega t}\right\} \tag{3.21}$$

The tilde and capitalisation of variables indicates definition in wavenumber domain ξ and in angular frequency domain ω. The displacement of the continuum gives rise to a transformed stress $\tilde{T}_{rz}(\xi,\omega)$ on the outer surface of the column. A transformed force per unit length $\tilde{F}_{rz}(\xi,\omega)$ is obtained by integrating the stress over the circumference f the column

$$\tilde{F}_{rz}(\xi,\omega) = \int_0^{2\pi} \tilde{T}_{rz}(\xi,\omega)a d\theta = 2\pi a\tilde{T}_{rz}(\xi,\omega) \tag{3.22}$$

The force $\tilde{F}_{rz}(\xi,\omega)$ is related to the displacement $\tilde{U}_z(\xi,\omega)$ by

$$\tilde{F}_{rz}(\xi,\omega) = \tilde{K}_z(\xi,\omega)\tilde{U}_z(\xi,\omega) \tag{3.23}$$

where $\tilde{K}_z(\xi,\omega)$ is representing the vertical stiffness per unit length of the elastic continuum. It can be written

$$\tilde{K}_{rz}(\xi,\omega) = -2\pi\mathrm{a}[0\ 0\ 1][\mathbf{T}]_{r=a}[\mathbf{U}]^{-1}_{r=a}\left\{\begin{array}{c}0\\0\\1\end{array}\right\}. \tag{3.24}$$

where the matrices **U**, **T** are transform coefficient matrices (given in Appendix C).

The differential equation of the displacement of the column in space and time domain is

$$-EA\frac{\partial^2 u_z(z,t)}{\partial z^2} + m'\frac{\partial^2 u_z(z,t)}{\partial t^2} = f_0\delta(z)e^{\jmath\omega t} + f_{rz}(z,t) \tag{3.25}$$

with Youngs modulus E, cross-sectional area A and mass per unit length m', applied force f_0 at $z=0$ and force distribution f_{rz} from the soil. $\delta(z)$ is the Dirac delta function defined such that $\delta(\xi) = 1$ for all ξ.

The displacement of a infinite pile in the wavenumber domain is obtained by substitution with 3.22 and Fourier transform of 3.25

$$\tilde{U}_z(\xi,\omega) = \frac{f_0}{EA\xi^2 + \tilde{K}_z(\xi,\omega) - m'\omega^2} \tag{3.26}$$

and by taking the inverse Fourier transform the displacement in space domain is obtained:

$$u_z(z,t) = \frac{1}{2\pi}\int_{-\infty}^{\infty} \tilde{U}_z(\xi,\omega)\mathrm{e}^{\jmath\xi z}d\xi\mathrm{e}^{\jmath\omega t} \tag{3.27}$$

For simulating boundary conditions of a finite pile with length L in a half-space with a free surface at $z = L$ the mirror-image method is used. The infinite pile is subjected to twice the force P (Fig.3.5(a)) corresponding to a semi-infinite system with mirror image plane at $z = 0$. The stress σ at length L is then

$$\sigma = E\left(\frac{dY_1}{dz}\right)_{z=L} \tag{3.28}$$

where dY_1 is the displacement of the semi-infinite column (Fig.3.5(b)). The free end boundary condition at $z = L$ is achieved by applying an equal and opposite stress at $z = L$. This is done by placing scaled mirror-image sources $P* = -EA(du_z/dz)$ at $z = L$ and at $z = -L$ on the infinite column as shown in (Fig.3.5(c)). The two forces on the infinite column correspond to a semi-infinite column with one force $P*$ acting at $z = L$ producing a stress

$$\sigma = E\left(\frac{dY_2}{dz}\right)_{z=L} = \frac{P*}{A} \tag{3.29}$$

where Y_2 is the displacement of the semi-infinite column shown in Fig.3.5(d). The stress is scaled to be equal and opposite of original load P so that

$$\left(\frac{dY_1}{dz}\right)_{z=L} = \left(\frac{dY_2}{dz}\right)_{z=L} \tag{3.30}$$

A force f_L, corresponding to displacements Y_1 and Y_2 gives rise to a displacement in space and time domain by eq 3.26 and 3.27. The response of a finite pile with two free ends and length L is then given by superposition of the displacement response from the semi infinite pile (see implementation chapter 4.3).

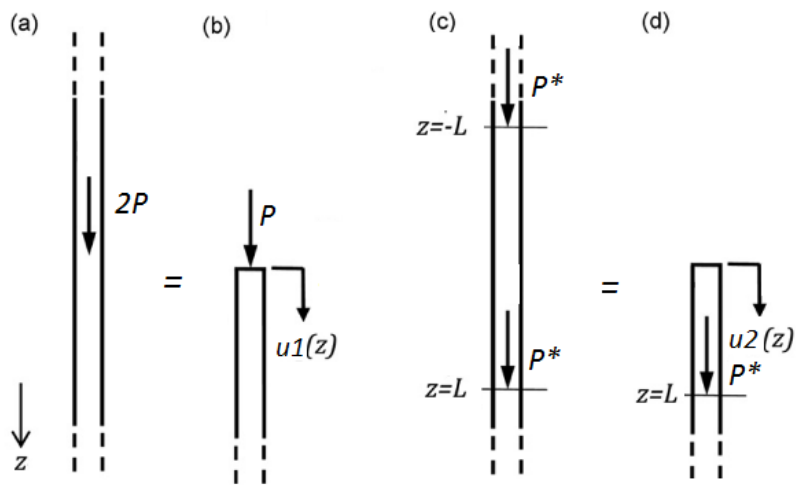

Figure 3.5.: Schematic procedure for simulating a finite pile with the mirror image method (based on [Kuo 13])

4. Implementation of the single pile

4.1. The layered ground implemented in FEM

An 3D solid model was built in *Comsol Multiphysics 4.3a* using the solid mechanics module [1].

4.1.1. Geometry

The geometry was drawn in a 2D work-plane which was revolved 90 degrees around the symmetry axis (in center of the pile) making a quarter cylinder (see figure 4.2). The geometry of a cylinder pile with length L and radius $d = 0.5m$ and layers of crust and clay (thickness $D_{crust} = 1.6m$, $D_{clay} = 80m$ and width $R = 60m$) with 2 corresponding PML-domains (having width $R_{PML} = 30m$) were drawn using a Cartesian coordinate system. Three data points were defined (see table 4.1).

Table 4.1.: Points in the FEM-geometry given in cylindrical coordinates

point	A	B	C
r [m]	0	50	50
z [m]	0	0	-30

4.1.2. Material properties

The single pile is a typical cylinder shaped concrete pile having material properties presented in table 4.2. Material damping in the pile is neglected.

The elastic properties in the ground are a function of the overburden pressure as explained in section 2.2. The ground prominently consists of a clay layer with properties presented in Table 4.3. The top layer is a dry crust with isotropic material properties and the botton bedrock is considered rigid.

[1] Attempts to implement an 2D-axisymmetric model failed because excitation in the axi-symmetric axis using point load is not implemented in the program. According to the software support it will be possible to apply point loads on the symmetry axis of a 2D axi-symmetric model in an upcoming release.

Table 4.2.: Material properties of the pile used in the model

Material	Youngs modulus E [Pa]	Density ρ [kg/m^3]	Poissons Ratio μ
Concrete pile	$37 * 10^9$	2700	0,3

Table 4.3.: Material properties of the soil used in the model. Values taken from in-situ measurement at Gamla Ullevi (from Norconsult Fältgeoteknik)

Material	Depth z [m]	Shear module G [MPa]	Density ρ [kg/m^3]	Poissons Ratio μ
Crust	0	28,35	1800	0,3
Clay	1,6	9,15	1560	0,4986
Clay	6,6	12,93	1570	0,4981
Clay	11,6	16,71	1580	0,4976
Clay	16,6	20,49	1600	0,4971
Clay	21,6	24,27	1610	0,4966
Clay	26,6	28,05	1630	0,4961
Clay	31,6	31,83	1640	0,4956
Clay	36,6	35,61	1660	0,4951
Clay	41,6	39,39	1670	0,4947
Clay	46,6	43,17	1680	0,4942
Clay	51,6	46,95	1700	0,4937
Clay	56,6	50,73	1710	0,4933
Clay	61,6	54,51	1730	0,4928
Clay	66,6	58,29	1740	0,4924
Clay	71,6	62,07	1760	0,4920
Clay	76,6	65,85	1770	0,4915
Bedrock	81,6	-	-	-

Based on measurement points at different levels presented in Table 4.3 the following interpolated functions are used for the material properties for clay ($z \geq 1.6$ meter) in the finite element model:

$$\begin{aligned} E_{soil} &= (18.78 + 2.246 \cdot z) \cdot 10^6 \qquad [Pa] \\ \rho_{soil} &= 1548 + 2.8 \cdot z \qquad [kg/m^3] \\ \mu_{soil} &= 0.4987 - 9.4598 \cdot 10^{-5} \cdot z \qquad [-] \end{aligned} \tag{4.1}$$

Youngs modulus and density is increasing with depth while Poissons ratio is decreasing slightly. The clay is saturated giving a nearly incompressible characteristics (similiar to water) and a Poissons ratio very close to 0.5. As a consequence the pressure wave speed is, like water, about 1500 m/s (see Fig.4.1). Material damping is included as a structural loss factor $\eta = 2 \cdot \xi = 0.02$ for both shear wave and pressure wave and the crust and the clay.

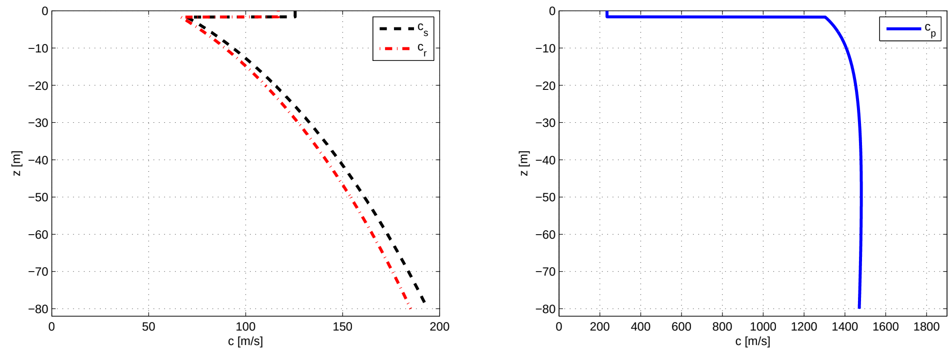

(a) Shear and Rayleigh wave

(b) Pressure wave

Figure 4.1.: Calculated wave speeds, c_p, c_s and c_r, as a function of depth z at the Gamla Ullevi site.

4.1.3. Boundary conditions

The pile is excited at its head in vertical direction (z-direction) by a harmonic force of 1 N distributed over the pile head surface (boundary load). Top area of the pile and top area of the crust are free boundaries i.e. no constrains or loads on the nodes in these layers. The bottom of the soil is a fully constrained boundary i.e. all nodes in the boundary have zero displacement in all directions. The two side walls adjacent to the pile have symmetric constrains which adds a boundary condition free in the plane and fixed in the out-of-plane direction representing symmetry in geometry and load. The two distant side walls have perfectly matching layer (PML) domain representing an open boundary (see section 3.4.3). One PML-domain for the crust and one for the clay was implemented defined in cylindrical coordinates, having typical wavelength equal to the shear wave speed ($\lambda = c_{s,crust}/f$ and $\lambda = c_{s,clay}/f$). The scaling factor F and the PML order n was by default set to 1.5. The center of rotation of the cylindrical PML-layer was in symmetric center z-axis. The performance of the PML was acceptable having at least 50 dB attenuation.

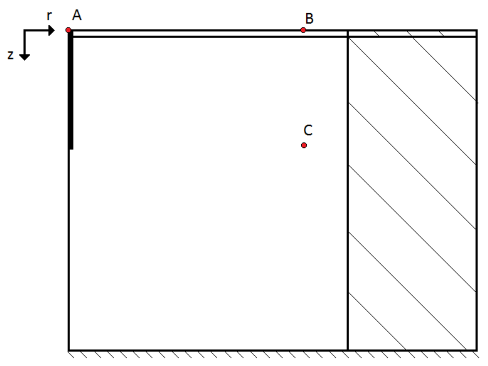

(a) Geometry

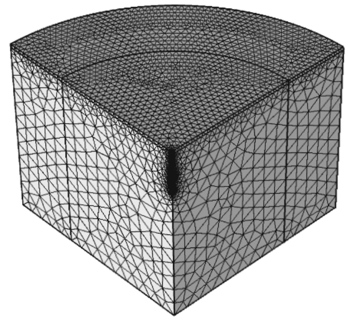
(b) Mesh

Figure 4.2.: The FEM model with ground properties for Gamla Ullevi

4.1.4. Mesh

Free tetrahedral elements were used on all domain. Governing for the element size was

- Elements in the pile domain small enough to capture the curvature of the circular pile side. The length between nodes in the pile is about 0,05 meters at the pile surface and about 0,2 meters at pile center.
- Elements in the PML-domain small enough for the performance of the PML. The maximum length between nodes in the PML domain is about 5 meter.
- Elements in the crust small enough to capture the shortest Rayleigh wavelength. Max length between nodes in the crust domain is about 2 meter.
- Elements in the clay small enough to capture the shortest shear wavelength. The length between nodes in the clay are about 0,1 meters at the pile surface and about 8 meters far from the pile.

4.2. The semi-infinite system

The site specific model described in section 4.1 is simplified to an idealized isotropic half sphere system to compare with the wavenumber model and the Robertson equation 3.10. The crust and the rigid bedrock floor are removed, and an eight of a sphere, consisting of clay layer and a PML layer, is added. The clay quarter cylinder around the pile has length L. When $L = 0$ i.e. no pile the model is compared with Robertsons equation 3.10.

The material was implemented as isotropic clay simply by using equations 4.1 with $z = 20m$. In this way the authentic clay could idealized as isotropic medium but still have similar material properties. The properties are shown in table 4.4.

Table 4.4.: Material properties for isotropic soil

Soil type	E_{soil} [MPa]	ρ_{soil} [kg/m^3]	μ_{soil}	c_p [m/s]	c_s [m/s]	c_r [m/s]
Gothenburg clay z=20m	63.7	1604	0.4968	1453	110	115

Two PML-domains having clay properties were used: One cylindrical PML-layer with center of rotation at the z-axis $(x, y) = (0, 0)$ and one spherical PML layer having center of rotation a the tip of the pile $((x, y, z) = (0, 0, -L))$. The settings on the PML were according to section 4.1.3 with the difference of the spherical PML having a typical wavelength representing the pressure wave $(c_{p,clay}/f)$.

The meshing and mesh sizes follow the criteria in section 4.1.4.

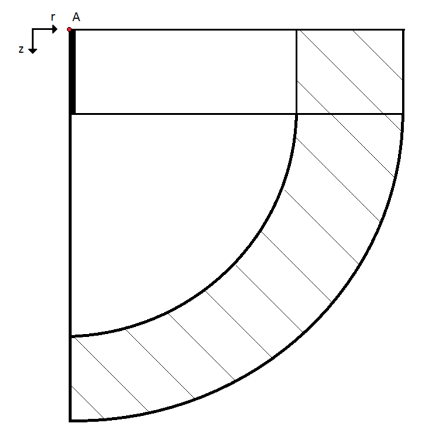

(a) Geometry

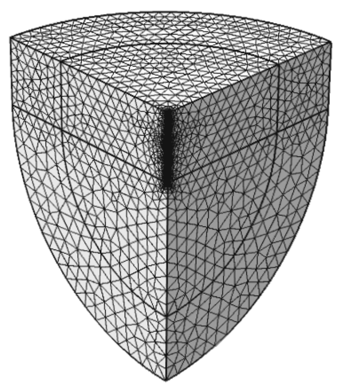
(b) Mesh

Figure 4.3.: The idealized half sphere model

4.3. Implementing the wavenumber model

The wave number model explained in section 3.5 was implemented in Matlab (see ref appendix D). For each frequency in the range 1 Hz to 20 Hz an array of wavenumbers was calculated. The spatial resolution dz was 0.01 m to capture the small wavenumbers involved and the number of elements in the spatial vector N were chosen so the length of the pile would be captured, see table 4.5.

Table 4.5.: Spatial partition of wavenumber model

Pile length [m]	5	10	20	30	40	50	80
number of elements N	2048	2048	4096	8192	8192	16384	16384

Material damping of the soil is included in the model according to

$$\begin{aligned} c_1^* &= c_1(1 + \jmath 2\beta_1) \\ c_2^* &= c_2(1 + \jmath 2\beta_2) \\ \lambda* &= \lambda(1 + \jmath 4\beta_1) \\ \mu* &= \mu(1 + \jmath 4\beta_2) \end{aligned} \tag{4.2}$$

where β_1 and β_2 are hysteresis material damping ratio for the pressure wave and shear wave respectively.

For each frequency and each wavenumber the displacement in wavenumber domain $\tilde{U}_{rz}(\xi, \omega)$ is calculated according to equation 3.26 with $f_0 = 2N$ for the finite pile case. The displacement in spatial domain is calculated with equation 3.27 implemented with *ifft*-command in Matlab.

The element in the spatial vector z corresponding to $z = L$ is calculated by the *find*-command. The displacement is calculated by taking the difference of adjacent elements in the vector d_u divided by $2dz$. The corresponding force representing the mirror image forces is $P^* = -EA(du_z/dz)$. The wavenumber field created by the two mirror image sources is

$$f_L = P^* \cdot e^{\jmath\xi L} + P^* \cdot e^{-\jmath\xi L} \tag{4.3}$$

The response in the spatial domain of the mirror image sources (calculated by 3.26 and 3.27 for f_L) is superposed on the response from the original force of the infinite pile (with f_0). The response at the excitation point $z = 0$ of a finite pile with length L is the element corresponding to $z = 0$ in the spatial displacement field vector. See Appendix D for Matlab-script.

5. Results

5.1. Validation of FEM model

The FEM-model is validated by comparing the point mobilities with the analytical expression by Robertson 3.10 (see figure 5.1(a)). The semi-infinite FEM model, with soil settings according to table 4.4, is excited by a boundary load with total force 1 N at a circular surface area with radius $a = 0.5\text{m}$. The mobilities show excellent agreement, the ripples at frequencies above 12 Hz is probably due to insufficient mesh-size in the the FEM-model. This result is also a validation of the symmetry boundary condition of the model i.e. the quarter cylinder (or sphere) model is representative for a full cylinder (or sphere) model.

The FEM-results agrees well with the Kuo & Hunt model for the isotropic clay, see figure 5.1(b). The discrepancy is at most 3 dB at low frequencies for shortest pile length and about 0.5 dB for medium length.

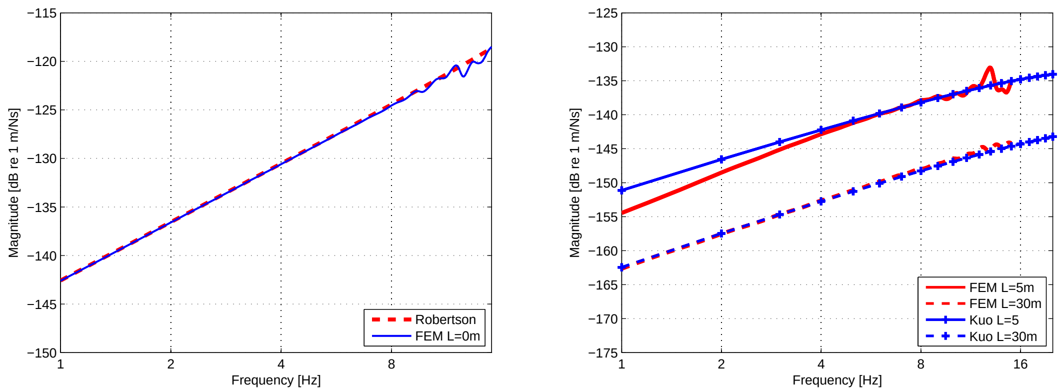

(a) Comparison Robertsons equation

(b) Comparison Kuo & Hunt

Figure 5.1.: Validation of FEM model on theory and wavenumber model

The reciprocity of the model is examined by comparing transfer mobilities between point A and point B (see table 4.1) in the layered model with piling length $L = 30\text{m}$. The transfer functions show perfect agreement as expected (see figure 5.2(b)). The result is interesting for conclusions on optimal piling depth against surface ground borne vibrations excited at a distance.

The stationary solver was used to calculate the static response of the layered model for different pile lengths L. Comparison in figure 5.2(b) with the dynamic response for highest and lowest frequencies show vertical displacement at the pile top decreasing with increasing pile length, as expected. A convergence behavior is seen in the static response as for the dynamic response. The static and low frequency dynamic response are converging with increasing pile length. The higher frequencies have less response and converge at a shorter pile length, compared to lower frequencies (f=15 Hz at L=25m as seen in figure 5.2(b)).

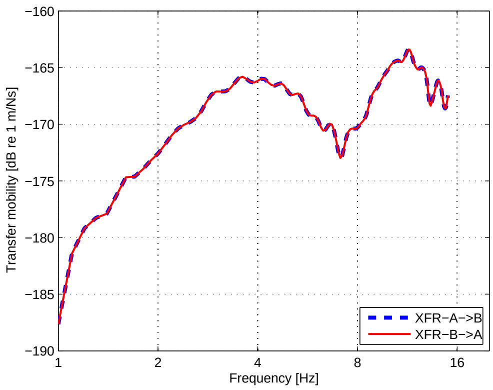

(a) Reciprocity validation

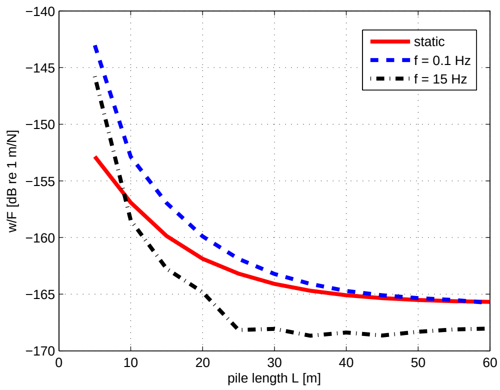

(b) Static comparison

Figure 5.2.: Validations of the FEM model

The wave energy radiated from a surface excitation is highest at the surface due to the Rayleigh wave and in the shear window (seen in 3.2). This is clearly seen in figure 5.3(a) where the total displacement field (considering all directions) is plotted for isotropic clay at $f = 10Hz$.

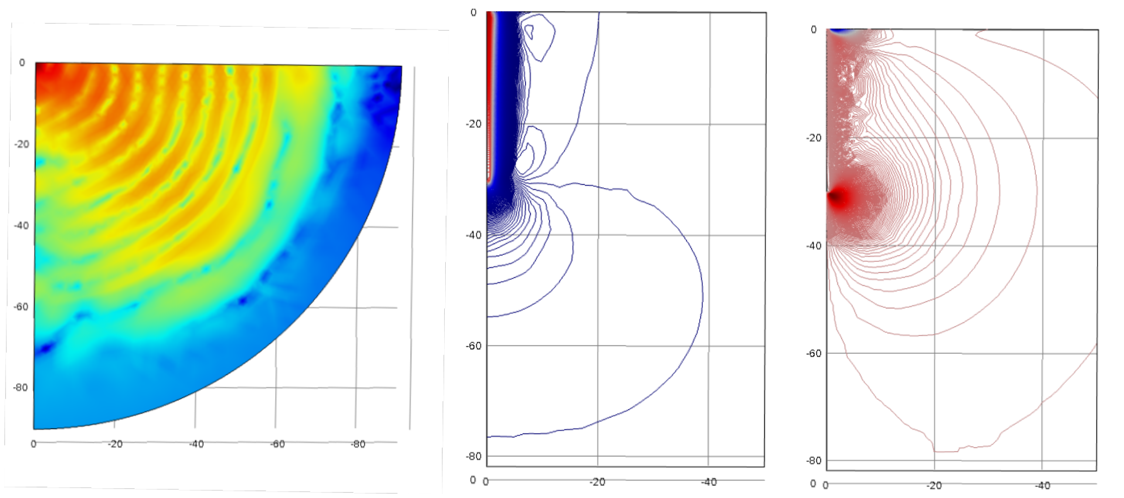

(a) shear window (b) Vertical displacement (c) Horisontal displacement

Figure 5.3.: Color and time plots of displacement field from FEM-model

In 5.3(b) and (c) is the vertical and horisontal displacement field at time t=0.05 s with 1000 isobars plotted. The isobars are evenly distributed from highest to lowest displacement value. The vertical displacements are in the order of ten times higher than the horizontal (not shown in figure). The soil is isotropic and pile length L=30m. The most distant isobar from the pile tip for horisontal displacement at 70 meters in 5.3(c) indicating the pressure wave front giving a pressure wave speed c_p of about 1400 m/s. For the vertical displacement in 5.3(b) the shear wave front can be seen at 7 meters distant from the pile length indicating a shear wave speed c_s at about 140 m/s.

5.2. Point mobilities

The results of the dynamic pile response are presented in point mobility magnitude $20 \cdot \log_{10} \frac{\frac{|\jmath\omega\hat{w}|^2}{F}}{Y_{ref}}$ where $Y_{ref} = 1m/Ns$ and phase $\tan^{-1}\left[\frac{Im\{\jmath\omega\hat{w}\}}{Re\{\jmath\omega\hat{w}\}}\right]$ over a frequency range from 1 Hz to 20 Hz in logarithmic scale. The input force is $F = \hat{F} \cdot e^{(\jmath\omega t)}$ where $\hat{F} = 1N$. Pile lengths vary from no pile L=0 to end bearing pile L=end (welded to rigid bedrock bottom) with interval of 5 meters i.e. L=(0:5:81.6). Representative lengths are presented in figure 5.4.

The shape of the mobility functions in fig 5.4 (a) and (b) is as expected i.e. having the frequency dependence mentioned in chapter 3.3. The magnitude of the mobility has an increase of about 6 dB per octave indicating spring mobility and stiffness behavior. For the shortest piles, L=0 and L=10, the increase per frequency is slightly lower above 4 Hz indicating damping behavior at higher frequencies (seen in 5.4(b)). For longer piles the response is stiffness dependent in the considered frequency range (see in Appendix A.1.1).

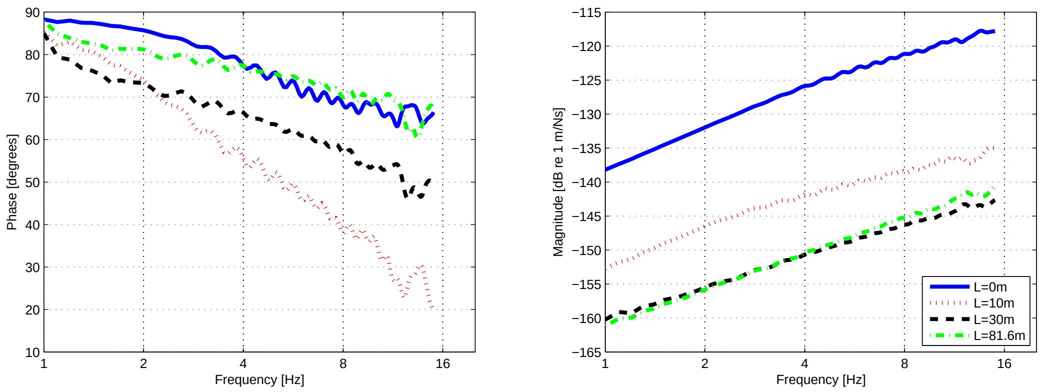

(a) Phase (b) Magnitude

Figure 5.4.: Point mobility response functions from FEM model

The ripples shown in the FEM model is probably due to interference from the vertical bedrock reflection and at highest frequencies insufficient mesh size might affect the accuracy.

Convergence of the response seem to be at a piling length of about 30 meters for the FEM model. The results for the isotropic FEM model and the Kuo & Hunt model wavenumber model is presented in the appendix A.1.2. The Kuo & Hunt model having isotropic material properties indicating that the convergence pile depth is not depending on isotropic or orthotropic soil. The response is governed by the soil properties and increasing pile length over 40 meters do not further reduce the response significantly.

The phase showing close to 90 degrees at lowest frequencies indicates spring mobility. The phase decreases with frequency; the damping increases and the stiffness decreases. The surface excitation (L=0m) show as stiff response as the longest pile. Since only the stiffer crust is excited this behavior is expected and can not be seen in fig 5.4(c) where the crust is absent. For longer piles the crust has little influence on the behavior and the crust is only following the motion i.e. inertial interaction.

The pile eigenfrequencies are assumed to be higher than the frequency range of interest (lowest resonance for pile with length L=50m is 40 Hz).

5.3. Transfer mobilities

The response results at points B and C is presented in transfer mobility magnitude for different pile lengths and the phase response of a pile with length L=30m. The magnitude of the mobility converges at a pile length about L=30 meter for both point B and point C.

At point C the response is about 10 dB to 15 dB smaller than the surface point B for converged piles (L>30m). At z=30 m the R-wave is not as dominant compared to surface point B allowing for bulk waves to be detected. Destructive interference with reflected pressure waves from bedrock is a probable reason for the dips in the response in point C (5.5 (d)) for higher frequencies.

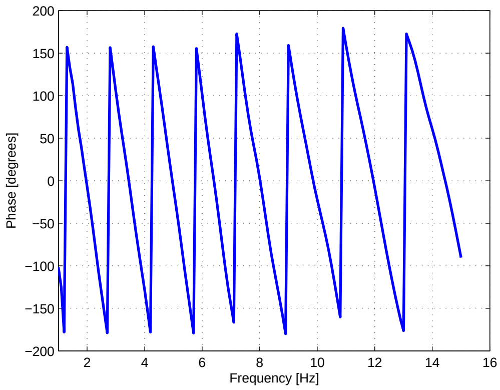

(a) Phase (r,z)=(50,0)m L=30m

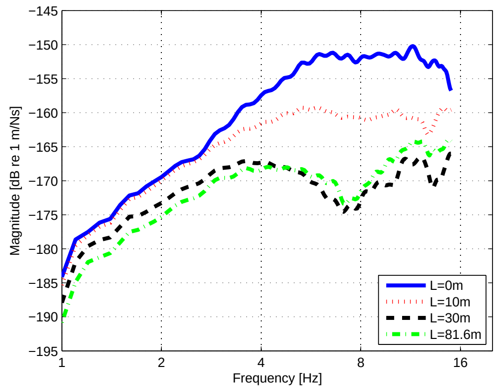

(b) Magnitude (r,z)=(50,0)m

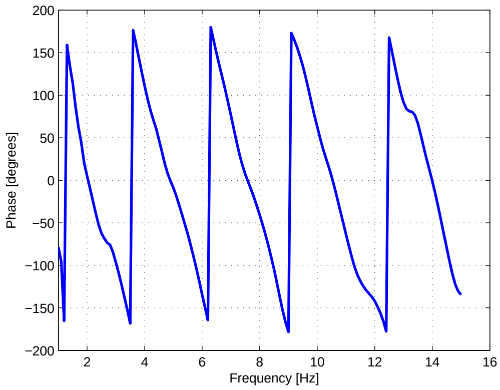

(c) Phase (r,z)=(50,-30)m L=30m

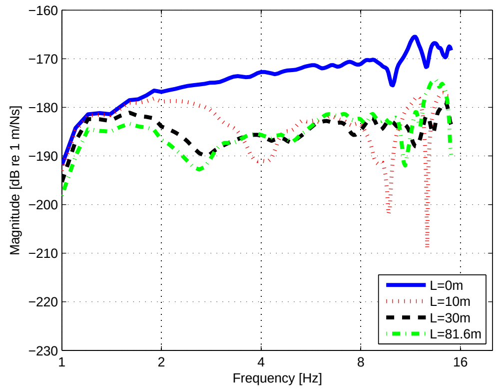

(d) Magnitude (r,z)=(50,-30)m

Figure 5.5.: Transfer functions of dynamic response

The transfer functions in figure 5.5 (b) indicate high response at frequencies f>4Hz for pile lengths L<20m can be explained by the presence of the Rayleigh wave. Piles with L<20m are good radiators (i.e. $Re\{Y\} > Im\{Y\}$) for frequencies f>4 Hz (See figure A.2(b) and (c) in Appendix A.1.1). The depth z of the R-wave motion, assuming $c_R = 80m/s$ and f>4Hz, is less than $z = 20m$. Piles shorter than 20 meters excite the Rayleigh wave.

From a phase spectra of a transfer function the phase wave speed c_{ph} is graphically calculated by the relation $c_{ph} = x\frac{df}{p}$ where x is the distance in m between the source and receiver, df is the frequency interval in Hz between two frequency points with equal phase (e.g. zero) and p is the number of full cycles between the points. The wave phase speed at surface seems constant at around 80 m/s (see table 5.1). Comparison with figure 4.1 shows decent agreement with shear wave and Rayleigh wave speeds for the top clay layer indicating that the movement of the crust is govern by the top clay layer.

The wave phase speed at depth z=30m is increasing with pile length, varying from 120 m/s to 174 m/s, indicating a dominant shear wave compared to the pressure wave. The distance x is from receiver point C to half pile length. The variations can be due to refraction phenomena and longer piles coupling to stiffer soil. The wave speeds agree well figure 4.1.

Table 5.1.: Wave phase speed calculated from transfer functions phase spectra

Pile length L [m]	0	10	20	30	40	50	end
c_{ph} point B [m/s]	82	80	80	81	82	81	85
c_{ph} point C [m/s]	120	125	133	153	153	174	174

6. Discussion

When increasing the pile length (i.e. increasing the pile slenderness), the stiffness of the pile, relative to the stiffness of the soil volume in contact with the surface of the pile, decreases. The soil creates a pressure on the pile side surface (radial direction) which causes shear forces at the pile/soil interface. These forces acts as a spring for lower frequencies and a damper for higher frequencies. The transition zone occurs at higher frequencies when increasing pile length.

The energy distribution into wave types, deduced for a surface excitation by a footing (see figure 3.2), is most likely changed when the footing is immersed into the soil corresponding to a pile with increasing length. From the transfer function results it is assumed that the energy part from the Rayleigh wave is decreased. The shear wave part is most likely increased in energy ratio since more shear forces are involved when increasing the pile length. The energy distributed by a pressure wave is probably about the same (however, higher in saturated clay than in theory example).

If considering the pile as a radiator an increase of the pile surface area would indicate a more powerful energy radiation. In that case; the real part ratio of the mobility would increase with pile length. Since it is the imaginary part ratio which increase with pile length, and the magnitude of the point mobility is governed by the imaginary part, the total radiated energy decreases.

Piles shorter than 20 meters radiate wave energy at frequencies above 4 Hz which causes up to 25 dB increase in vertical surface vibration levels at 50 meters distance compared to foundations deeper than 30 meters. If a point at longer distance would have been analyzed, even lower frequencies would have been detected as radiated. Piles shorter than 20 meters have inertial interaction with R-wave. Piles longer than 20 meters have kinematic interaction withstanding the R-wave.

The frequency transition zone where the real part of the mobility starts to dominate over the imaginary part is governed by the size of the pile. This transition is interpreted as corresponding to Helmholtz number 1. A larger pile diameter results in the Helmholtz number decreases in frequency i.e. longer wavelengths are excited.

The transverse isotropic layered soil model corresponds to an isotropic soil model at z=20m which is expected considering that 20 meters level is roughly at about half the pile length when converging i.e. the total shear force that the pile exhibits is about the same.

The surface Rayleigh wave is detected in the phase response function at 50 meters having a speed of 80 m/s indicating that the crust is only following the motion governed by the top clay layer. The bulk shear wave detected at 30 meters depth is increasing in speed with increasing pile length which is probably due to refraction and coupling with stiffer layers. The pressure wave front is detected in a time plot for horizontal displacement having a speed of 1400 m/s.

The results, which are generated by implementing fixed geometry and frequencies in the model, indicate a relation which can , and should, be extended into geometrical relations and wavelengths.

7. Conclusions

Ground vibrations is a subject field which is gaining attention lately both from health, environmental and engineering research. A background study on ground vibrations and a literature survey on dynamic response of pile/soil system is conveyed.

The purpose of this thesis is to find an optimal piling depth in clay, regarding the pile foundation both as the vibration source and aldo as a recipient subjected to vibrations excited at a distance.

Finite element models are built up and used to study the dynamic response of the vertically excited single pile and driving point and transfer mobility and phase functions are analyzed. The soil types are one layered case-specific clay with depth dependent parameters and one isotropic clay.

The accuracy of the FEM model is validated by perfect agreement in comparison with a known expression for dynamic response of an elastic halfspace. Comparison with an up-to-date wavenumber model for dynamic response of a single pile published by Kuo and Hunt (2013) shows good agreement. The FEM model is also validated in frequency and time domain of the wave field behaving as predicted.

The FEM model show a convergence depth of about 30 meters for a cylindrical pile with radius 0.5 meter in transverse isotropic layered clay. Both FEM model and wavenumber model shows similar result for isotropic clay.

Some concluding remarks of the results found in this study are:

- The pile response in the FEM models is decreasing with increasing pile length until convergence depth at about 30 meters. Both point mobility results for four different soil properties and transfer mobility results indicate that piling depth over 30 meters will not significantly improve the dynamical axial stiffness of a pile with a diameter of 1 meter. Since the reciprocity assumption is valid the conclusion is that pile foundations subjected to ground vibrations have the same optimal piling depth.
- The response level at the convergence depth is similar for isotropic soil as for

the transverse isotropic layered soil indicating that z=20 depth level is a valid representative.

- The FEM model is validated against theory by perfect agreement with a known expression for dynamic response of elastic half-space. When analyzing time- and frequency result of the wave field the model agrees with predicted wave speeds and behaviors. Comparison with the wavenumber model show good agreement and the conclusion is that the FEM model is accurate in the frequency range of interest.

- When analyzing the transfer functions it is seen that over a certain frequency, piles shorter than 20 meters, seem to excite the Rayleigh surface wave while piles longer than 20 meters do not. The reciprocity of the transfer functions allow for the conclusion that piling further than 30 meters is not needed for anchoring a foundation subjected to surface excited ground vibrations.

Some results have been found in this study. Yet, there are more questions to be answered. A few of those are:

- The single pile is and an idealized system. Real building foundations are often pile groups or groups of pile groups which further increases the static loading capacity. The dynamic response and pile-soil-pile interaction is a complex study field where also radial, transverse and torsional motions need to be taken into account.

- Could the convergence depth detected in the models used in this thesis be seen in small or full scale tests or even in measurement?

- In this study the pile diameter is kept constant. It would be interesting to see how varying this parameter would influence the convergence depth. Expected result would be a shorter convergence pile length for smaller pile diameters i.e. the ratio d/L would be constant.

- Interesting would also be a more extended study on the distribution ratio of wave energy into the different wave types and how that ratio changes with Poissons number and length of pile.

References

[Mol 00] Möller, B. et al (2000): *Geodynamik i praktiken*, Information 17 - Swedish Geotechnical Institute (SGI), Linkoping

[Hal 12] Hall, L. et al (2012): *Markvibrationer*, SGF informationsskrift 1:2012, Swedish Geotechnical Gociety (SGF), SGF's markvibrationskommitt

[Erl 96] Erlingsson, S. Bodare, A. (1996): *Live load induced vibrations in Ullevi Stadium dynamic soil analysis*, Soil Dynamics and Earthquake Engineering 15 (1996) 171-188

[Wid 13] Widn, G. (2013) Mail correspondance with supervisor Gunnar Widn.

[Srb 10] Srbulov, M. (2010): *Ground Vibration Engineering - Simplified Analyses with Case Studies and Examples*, Springer Science+Business Media B.V. Springer Dordrecht Heidelberg London New York

[Sal 01] Sällfors, G. (2001): *Geoteknik : jordmateriallra, jordmekanik*, Goteborg: Vasastadens boktryckeri]

[Lam 04] Lamb, H. (1904): *On the Propagation of Tremors over the Surface of an Elastic Solid*, Transactions of the Royal Society of London. Series A, Containing Papers of a Mathematical or Physical Character, Vol. 203 (1904), pp. 1-42

[Ewi 57] Ewing W M, Jardetzky W S and Press F (1957): *Elastic waves in Layered Media*, McGraw–Hill, New York. 405 p.

[Ric 70] Richart, F.E., Woods R.D., Hall, J.R. (1970): *Vibrations of Soils and Foundations*, Prentice-Hall, Englewood Cliffs, N.J. 414 p.

[Nov 74] Novak M (1974): *Dynamic Stiffness and Damping of Piles*, Canadian Geotechnical Journal. Volume 11, Number 4, 1974, pp. 574598

[Nov 77] Novak M (1977): *Vertical response of floating piles*, Journal of the Engineering Mechanics Division, Vol. 103, No. 1, 1977, pp. 153-168

[Kay 91] Kaynia A M, Kausel E (1991): *Dynamics of piles and pile groups in layered soil media*, Soil Dynamics and Earthquake Engineering, Volume 10, Number 8, pp. 386-401

[Wug 97] Wu G, Finn W D L (1997): *Dynamic elastic analysis of pile foundations using finite element method in the frequency domain*, Canadian Geotechnical Journal. Volume 34 Number 1, pp. 34-43

[Aue10] Auersch L (2010): *Wave propagation in the elastic half-space due to an interior load and its application to ground vibration problems and buildings on piles*, Soil Dynamics and Earthquake Engineering Volume 30 pp. 925936

[Kuo 13] Kuo K A, Hunt H E M (2013): *An efficient model for the dynamic behaviour of a single pile in viscoelastic soil*, Journal of Sound and Vibration (2013)

[Ayo 12] Ayothiraman R, Boominathan A (2012): *Depth of Fixity of Piles in Clay Under Dynamic Lateral Load*, Geotechnical and Geological Engineering, published online december 2012, URL:

[Gla 68] Gladwell G M L (1968): *The calculation of mechanical impedances relating to an indenter vibrating on the surface of a semi infinite elastic body*, Journal of Sound and Vibration, Volume 8, Number 2, pp.215-228

[Rob 66] Robertson, I. (1966): *Forced vertical vibration of a rigid circular disc on a semi-infinite elastic solid*, Mathematical Proceedings of the Cambridge Philosophical Society, 62, pp 547-553

[Pet 83] Peterssen B (1983): *Studies of ordinary and effective mobilities for the determination of structure-borne sound power transmission*, 1983, Report, Chalmers university of technology, Department of building acoustics, ISBN 9170321116, Volym 457

[SIS 99] Swedish standard (1999): *Vibration and shock - Guidance levels and measuring of vibrations in buildings originating from piling, excavating and packing to estimate permitted vibration levels*, (In Swedish). SS 02 52 11. Swedish Institute for Standards, SIS, Stockholm 1999, 7 p.

[Gid 12] Gidlöf-Gunnarsson A, Ögren M, Jerson T, Öhrstrm E. (2012): *Railway noise annoyance and the importance of number of trains, ground vibration, and building situational factors.* Noise Health 2012;14:190-201)

[Cre 05] Cremer, L. Heckl, M. Petersson. B.A.T. (2005): *Structure-Borne Sound-Structural Vibrations and Sound Radiation at Audio Frequencies* 3rd edition Springer Berlin Heidelberg New York

[Num 06] (2006:)*Numerical methods - from Euler to FEM* TA2 course page URL: $http : //www.ta.chalmers.se/downloads/students/cpg_ta2/ta2_num_eul_fem.pdf$

[Com 12] Comsol (2012): *Structural Mechanics Module Users Guide* Comsol version 4.3a 19982012 COMSOL

[For 06] Forrest, J.A. Hunt, H.E.M (2012): *A three-dimensional tunnel model for calculation of train-induced ground vibration* Journal of Sound and Vibration 294 (2006) 678705

[Cou 10] Coulier, P. (2010): *The Vibration Response of Piled Foundations to Inertial and Underground Railway Induced Loadings* Masters Thesis, Katholieke Universiteit, Leuven URL: $http://www.scriptiebank.be/sites/default/files/39c7c9678f9481b70df851018f5a707c.pdfS.$

[Efu 13] (2013): *Transverse Isotropic Definition* Engineering fundamentals URL: $(http://www.efunda.com/formulae/solid_mechanics/mat_mechanics/hooke_iso_transverse.cfm)$

A. Mobility results

A.1. Point mobility results

A.1.1. Point mobilities layered Gothenburg clay

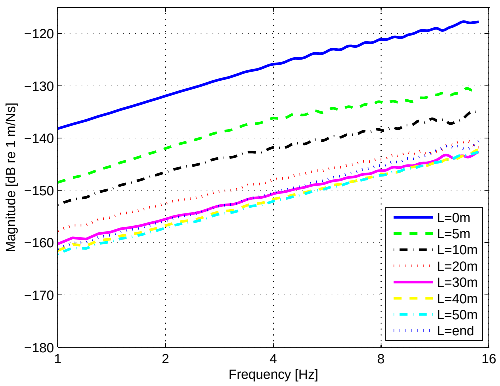

(a) Magnitude

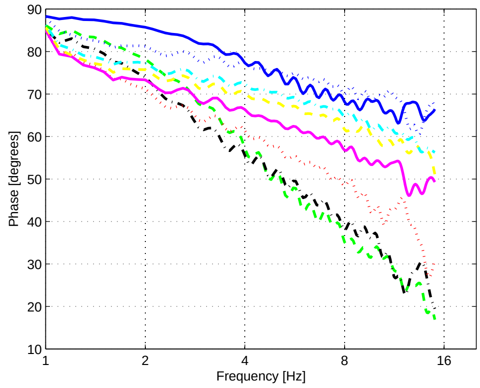

(b) Phase

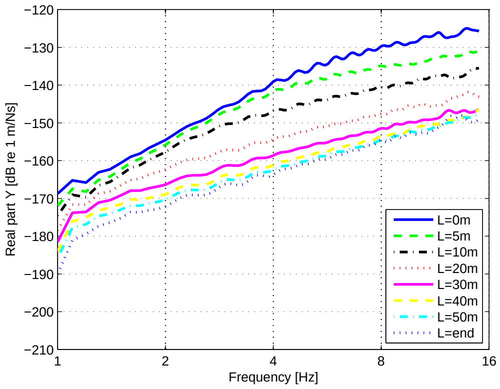

(c) Real part

Figure A.1.: Point Mobility FEM results with layered material parameters

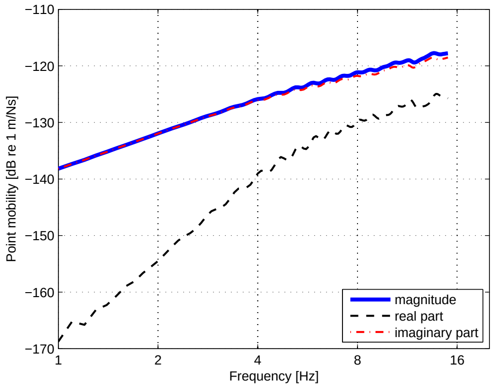

(a) L = 0m

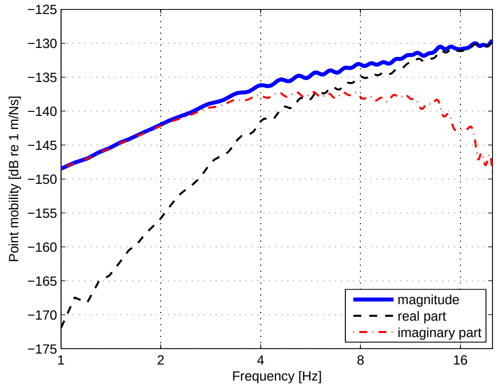

(b) L = 5m

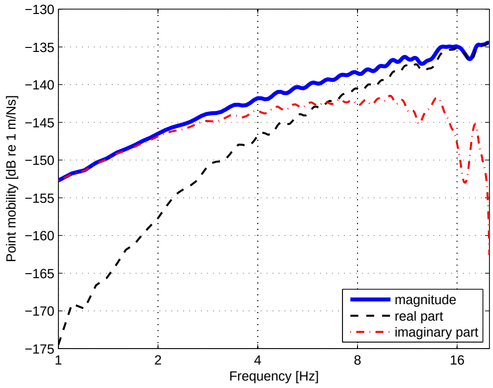

(c) L = 10m

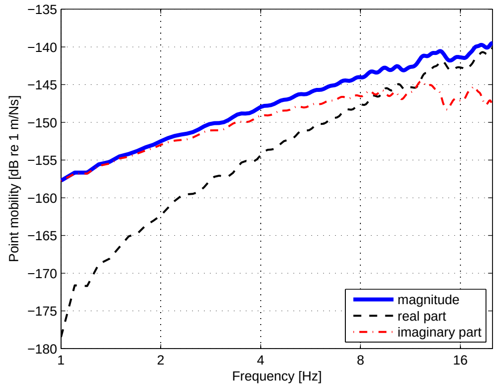

(d) L = 20m

Figure A.2.: Point Mobility FEM results for different lengths with layered material parameters

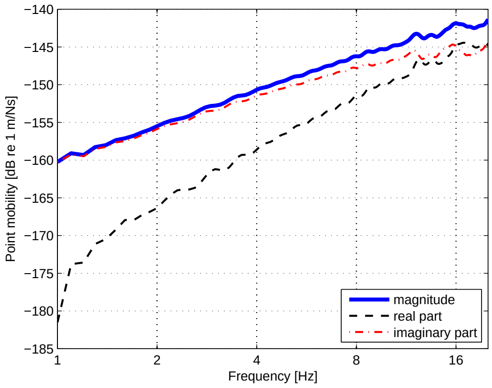

(a) L = 30m

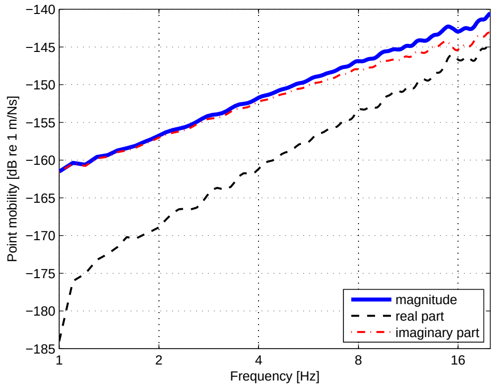

(b) L = 40m

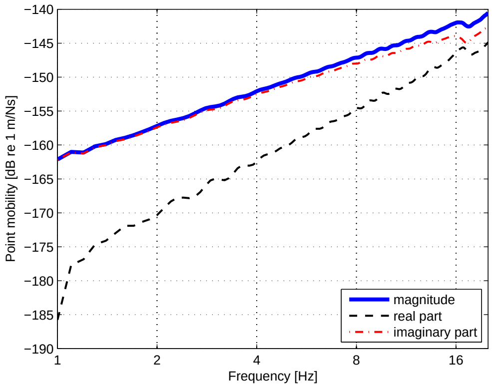

(c) L = 50m

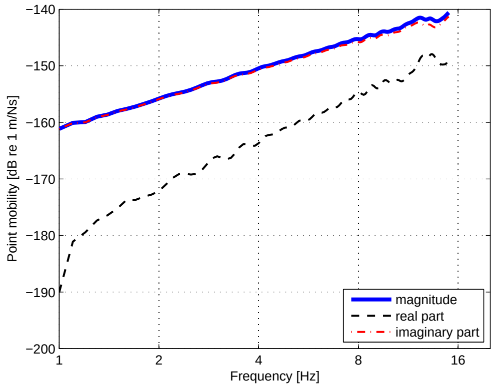

(d) L = end

Figure A.3.: Point Mobility FEM results for different lengths with layered material parameters

A.1.2. Point mobilities isotropic clay

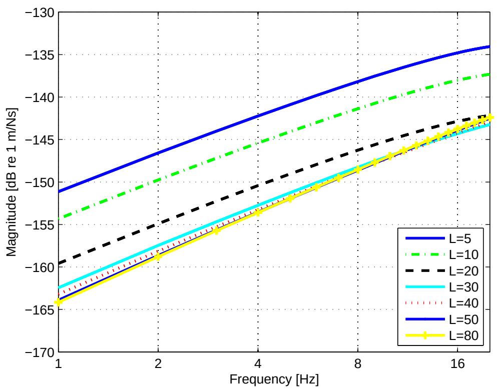

(a) Magnitude Kuo&Hunt

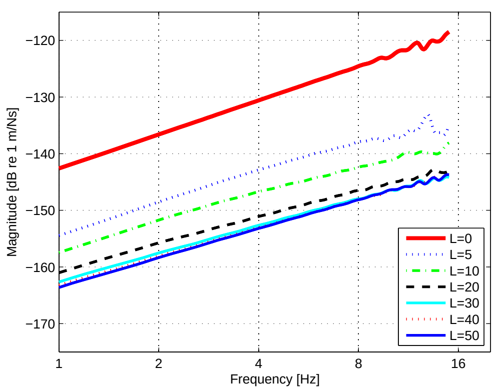

(b) Magnitude FEM

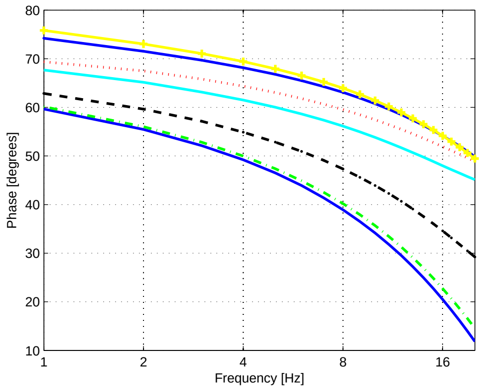

(c) Phase Kuo&Hunt

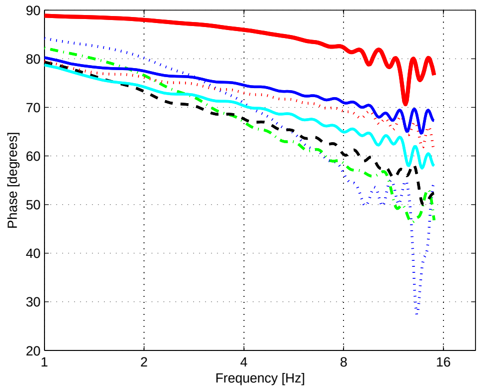

(d) Phase FEM

Figure A.4.: Point Mobility results isotropic clay

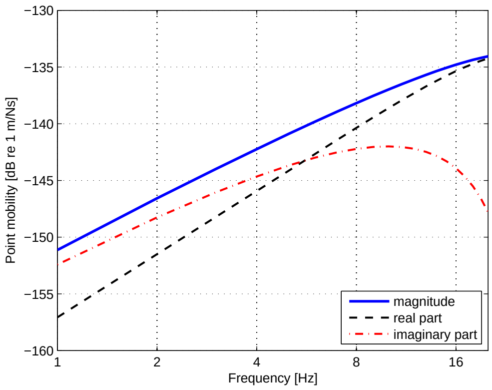

(a) Kuo&Hunt z=20m L = 5m

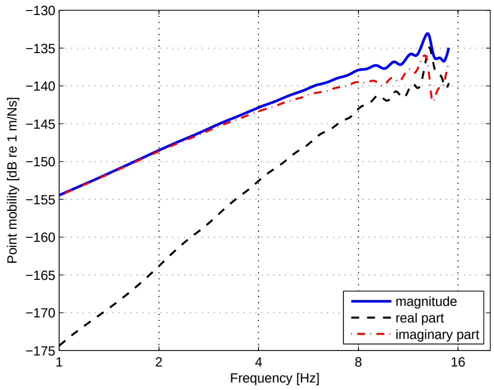

(b) FEM z=20m L = 5m

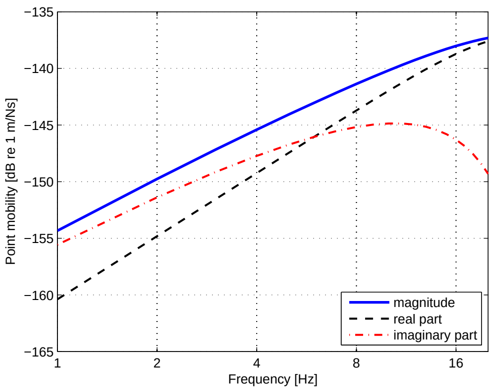

(c) Kuo&Hunt z=20m L = 10m

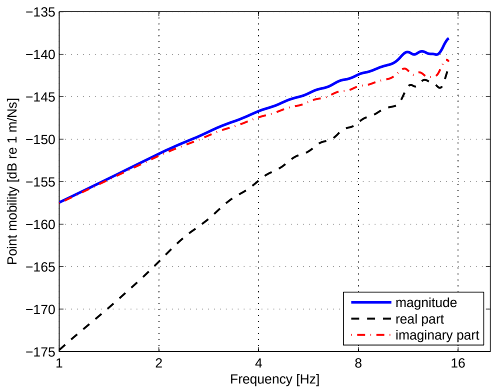

(d) FEM z=20m L = 10m

Figure A.5.: Point Mobility results isotropic clay

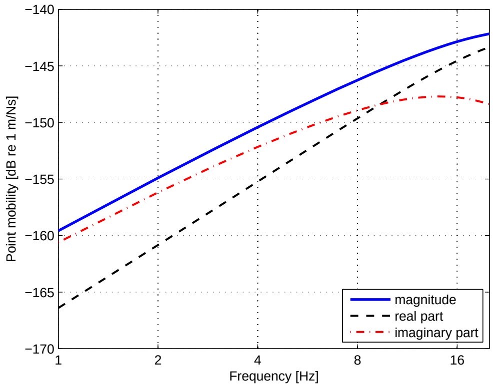

(a) Kuo L = 20m

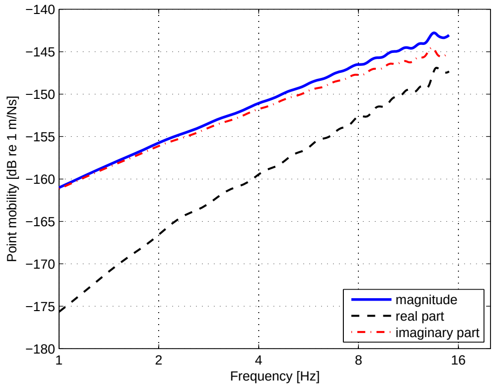

(b) FEM L = 20m

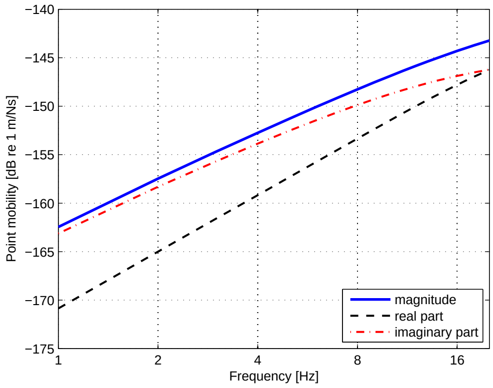

(c) Kuo L = 30m

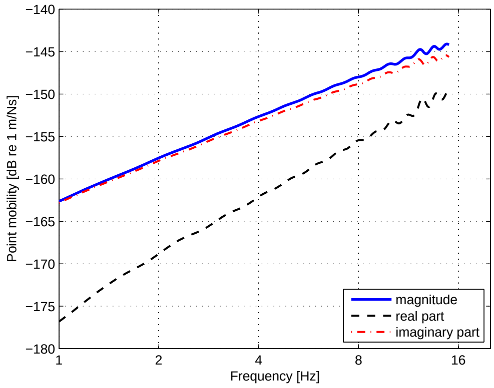

(d) FEM L = 30m

Figure A.6.: Point Mobility results isotropic clay

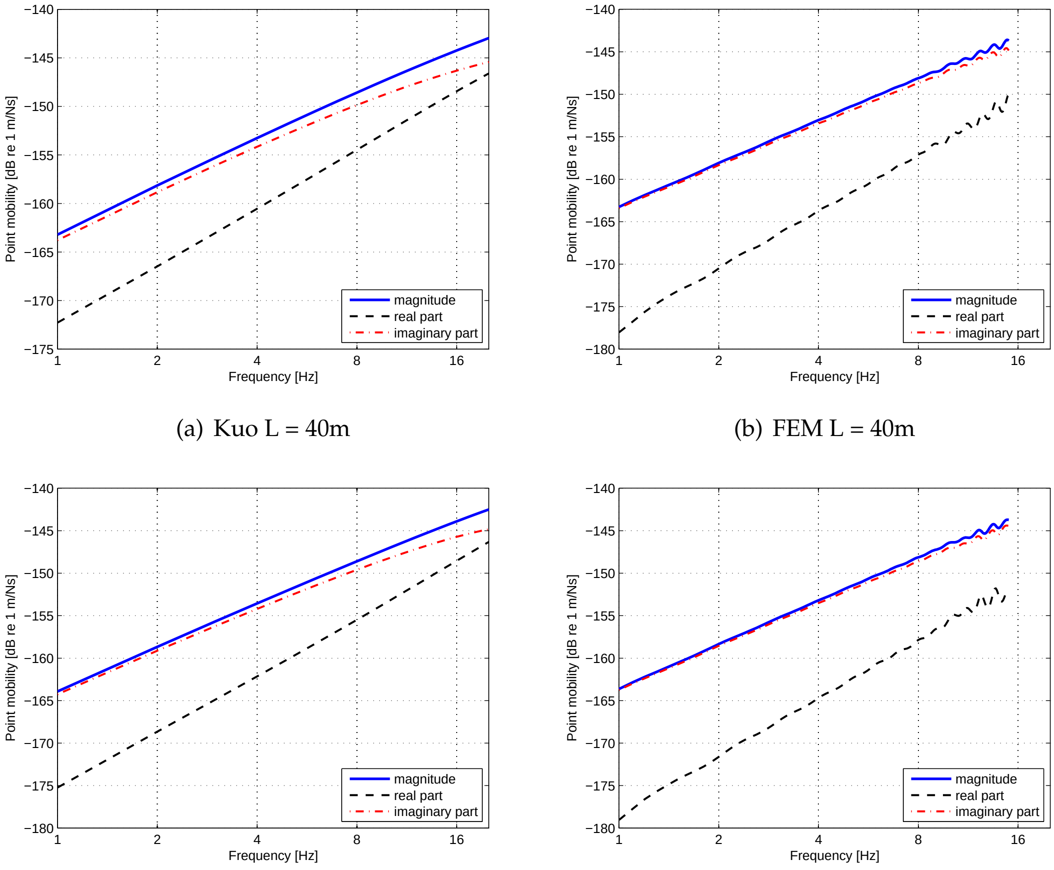

(a) Kuo L = 40m

(b) FEM L = 40m

(c) Kuo L = 50m

(d) FEM L = 50m

Figure A.7.: Point Mobility results isotropic clay

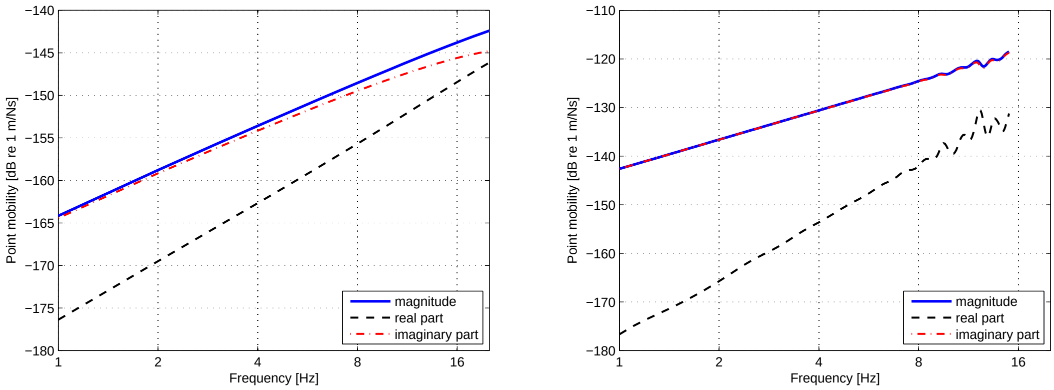

(a) Kuo L = 80m (b) FEM L = 0m

Figure A.8.: Point Mobility results isotropic clay

A.2. Transfer mobility results

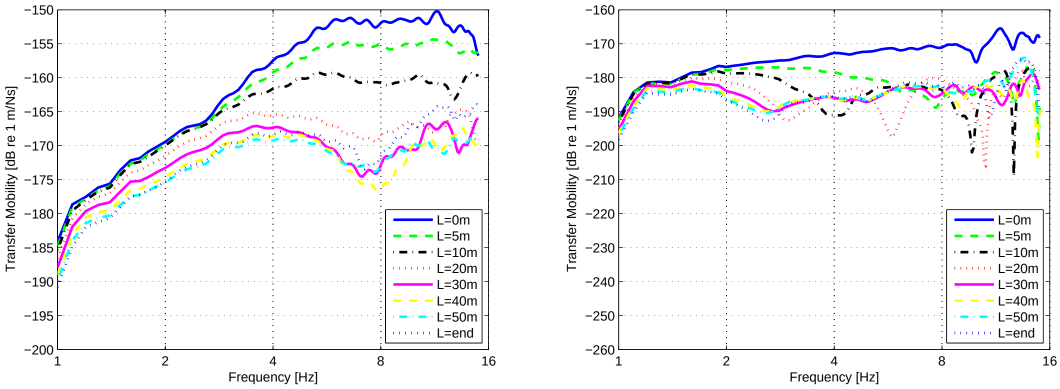

(a) Magnitude (r,z)=(50,0)m

(b) Magnitude (r,z)=(50,-30)m

Figure A.9.: Transfer Mobility FEM results with layered material parameters

B. Stiffness matrices

In the linear stress and strain relation $\{\sigma\} = [D] \cdot \{\epsilon\}$ the stress vector $\{\sigma\} = \begin{bmatrix}\sigma_x\ \sigma_y\ \sigma_z\ \tau_{xy}\ \tau_{xz}\ \tau_{yz}\end{bmatrix}^T$ where τ is the shear stress and the strain vector $\{\epsilon\} = \begin{bmatrix}\epsilon_x\ \epsilon_y\ \epsilon_z\ \gamma_{xy}\ \gamma_{xz}\ \gamma_{yz}\end{bmatrix}^T$ where γ is the shear strain. The stiffness matrix D depends on material properties and is explained below.

B.1. Elements of isotropic stiffness matrix

For an isotropic media the elasticity matrix is [Com 12]

$$\mathbf{D} = \frac{E}{(1+\mu)(1-2\mu)} \begin{bmatrix} 1-\mu & \mu & \mu & 0 & 0 & 0 \\ \mu & 1-\mu & \mu & 0 & 0 & 0 \\ \mu & \mu & 1-\mu & 0 & 0 & 0 \\ 0 & 0 & 0 & \frac{1-2\mu}{2} & 0 & 0 \\ 0 & 0 & 0 & 0 & \frac{1-2\mu}{2} & 0 \\ 0 & 0 & 0 & 0 & 0 & \frac{1-2\mu}{2} \end{bmatrix} \tag{B.1}$$

B.2. Elements of orthotropic stiffness matrix

The elasticity matrix for an orthotropic media is [Efu 13]

$$\mathbf{D} = \begin{bmatrix} D_{11} & D_{12} & D_{13} & 0 & 0 & 0 \\ D_{12} & D_{22} & D_{23} & 0 & 0 & 0 \\ D_{13} & D_{23} & D_{33} & 0 & 0 & 0 \\ 0 & 0 & 0 & D_{44} & 0 & 0 \\ 0 & 0 & 0 & 0 & D_{55} & 0 \\ 0 & 0 & 0 & 0 & 0 & D_{66} \end{bmatrix} \tag{B.2}$$

where the elements for the transverse isotropic case are

$$D_{11} = \frac{1-\mu_{pz}\mu_{zp}}{E_p E_z \nabla} \qquad D_{12} = \frac{\mu p + \mu_{zp}\mu_{pz}}{E_p E_z \nabla} \qquad D_{13} = \frac{\mu_{zp} + \mu_p \mu_{zp}}{E_p E_z \nabla}$$

$$D_{21} = \frac{\mu_p + \mu_{pz}\mu_{zp}}{E_p E_z \nabla} \qquad D_{22} = \frac{1-\mu_{zp}\mu_{pz}}{E_p E_z \nabla} \qquad D_{23} = \frac{\mu_{zp} + \mu_{zp}\mu_p}{E_p E_z \nabla}$$

$$D_{31} = \frac{\mu_{pz} + \mu_p \mu_{pz}}{E_p^2 \nabla} \qquad D_{32} = \frac{\mu_{pz}(1+\mu_p)}{E_p^2 \nabla} \qquad D_{33} = \frac{1-\mu_p^2}{E_p^2 \nabla}$$

$$D_{44} = 2G_{zp} \qquad D_{55} = 2G_{zp} \qquad D_{66} = \frac{E_p}{1+\mu_p} \tag{B.3}$$

where E_p and μ_p is the Youngs modulus and poissons ratio in the symmetric plane, E_z and μ_z is the Youngs modulus and poissons ratio in the z-direction, G_z is the shear modulus in z-direction and

$$\nabla = \frac{(1+\mu_p)(1-\mu_p - 2\mu_{pz}\mu_{zp})}{E_p^2 E_z} \tag{B.4}$$

and $D_{12} = D_{21}$, $D_{13} = D_{31}$ and $D_{23} = D_{32}$.

C. Transformation matrices for wavenumber model

In these equations $\alpha^2 = \xi^2 - \omega^2/c_1^2$, $\beta^2 = \xi^2 - \omega^2/c_2^2$, K_n are modified Bessel functions of the second kind of order n, λ and μ are Lame's constants, c_1 and c_2 are pressure and shear wave speeds in the medium, ω is the angular frequency and ξ is the longitudinal wavenumber [Kuo 13].

$$\mathbf{U} = \begin{bmatrix} u_{12} & u_{14} & u_{16} \\ u_{22} & u_{24} & u_{26} \\ u_{32} & u_{34} & u_{36} \end{bmatrix} \qquad \mathbf{T} = \begin{bmatrix} t_{12} & t_{14} & t_{16} \\ t_{22} & t_{24} & t_{26} \\ t_{32} & t_{34} & t_{36} \end{bmatrix} \tag{C.1}$$

with the elements

$$\begin{aligned}
u_{12} &= \frac{n}{r} K_0(\alpha r) - \alpha K_1(\alpha r) \\
u_{14} &= \jmath \xi K_1(\beta r) \\
u_{16} &= \frac{n}{r} K_0(\beta r) \\
u_{22} &= -\frac{n}{r} K_0(\alpha r) \\
u_{24} &= \jmath \xi K_1(\beta r) \\
u_{26} &= -\frac{n}{r} K_0(\beta r) - \beta K_1(\beta r) \\
u_{32} &= \jmath \xi K_0(\alpha r) \\
u_{34} &= \beta K_0(\beta r) \\
u_{36} &= 0
\end{aligned} \tag{C.2}$$

and

$$
\begin{aligned}
t_{12} &= -\lambda\xi^2 + (\lambda + 2\mu)K_0(\alpha r) + 2\mu\frac{\alpha}{r}K_1(\alpha r) \\
t_{14} &= -2\mu\jmath\xi\beta K_0(\beta r) - 2\mu\jmath\xi\frac{1}{r}K_1(\beta r) \\
t_{16} &= 0 \\
t_{22} &= 0 \\
t_{24} &= -\mu\jmath\xi\beta K_0(\beta r) - 2\mu\jmath\xi\frac{1}{r}K_1(\beta r) \\
t_{26} &= -\mu\beta^2 K_0(\beta r) - 2\mu\frac{\beta}{r}K_1(\beta r) \\
t_{32} &= -2\mu\jmath\xi\alpha K_1(\alpha r) \\
t_{34} &= -\mu(\xi^2 + \beta^2)K_1(\beta r) \\
t_{36} &= 0
\end{aligned} \tag{C.3}
$$

D. Matlab script for wavenumber model

```
%%%%%%%%%%%%%%%%%%%%%%%%%%%%%%%%%%%%%%%%%%%%%%%%%%%%%%%%%%%%

% Wavenumber domain model for single pile dynamic behavior
% after Kuo&Hunt 2013
% implemented by Erik Olsson and Patrik Andersson
% 2013-06-01

%%%%%%%%%%%%%%%%%%%%%%%%%%%%%%%%%%%%%%%%%%%%%%%%%%%%%%%%%%%%%%
clear all;tic

%%%%%%%%%%%%%%%%%%%%%%%%%%%%%%%%%%%%%%%%%%%%%%%%%%%%%%%%%%%%%%%
% Defining variables and vectors
%%%%%%%%%%%%%%%%%%%%%%%%%%%%%%%%%%%%%%%%%%%%%%%%%%%%%%%%%%%%%%%

% ..............................................................
% Frequency vector
f_vector=1:1:20;

% ..............................................................
% Spatial vector
dz=0.5;%0.01
Nz=1048;
z=((-Nz/2+1):Nz/2)*dz;

% ..............................................................
% Pile properties
rho_pile = 2700;%2700...2860;
E_pile = 37e9; %37e9...40e9
nu_pile = 0.3;%0.3...0.25
a = 0.5;A=a^2*pi;
L=30;%[5 10 20:10:50];
m_prim = rho_pile*A;

% ..............................................................
% Soil properties
rho_soil = 1604;%1604..1688...2000
G_soil = 21.28e6; %21.28e6..43.9e6....143e6    E=G(2(1+nu))
nu_soil = 0.4968; %4968..494....0.4
D=(G_soil*(2*(1+nu_soil)).*(1-nu_soil))./((1+nu_soil).*(1-2*nu_soil));
```

```
c_1 = sqrt(D/rho_soil); %Pressure wave speed
c_2 = sqrt(G_soil/rho_soil); % Shear wave speed
beta_1 = 0.04;beta_2 = 0.04;
% Lames material constants
lambda = 2*nu_soil*G_soil./(1-2*nu_soil)*(1+1i*4*beta_1);
mu = G_soil*(1+1i*4*beta_2);
% Wave speeds with damping
c_1_damp = c_1*(1 + 1i*2*beta_1);
c_2_damp = c_2*(1 + 1i*2*beta_2);

% ..............................................................
% Parameters for the eq. system
n=0; % Order of the Bessel functions (n=0: axial, n=1: transverse)
r = a; % Pile/soil boundary
f_0 = 2; % Excitation force

% ..............................................................
% Wavenumber vector
xsi_max=2*pi/(dz);%2*pi/dz;
xsi_vector=[(0:Nz/2) ((-Nz/2+1):1:-1)]*xsi_max/Nz;

%%%%%%%%%%%%%%%%%%%%%%%%%%%%%%%%%%%%%%%%%%%%%%%%%%%%%%%%%%%%%%%
% Setting up the eq.syst. and solve
%%%%%%%%%%%%%%%%%%%%%%%%%%%%%%%%%%%%%%%%%%%%%%%%%%%%%%%%%%%%%%%

% ..............................................................
% Allocating vectors
U_z = zeros(1,length(xsi_vector));
K_z = zeros(1,length(xsi_vector));
u_z_matrix = zeros(length(f_vector),length(xsi_vector));
u_zL_matrix = zeros(length(f_vector),length(xsi_vector));
u_zL_super = zeros(length(f_vector),length(xsi_vector));
U_xsi_matrix = zeros(length(f_vector),length(xsi_vector));
u_0=zeros(1,length(f_vector));
u_0_super=zeros(1,length(f_vector));
u_L = zeros(length(L),length(f_vector));

%..............................................................
% Looping over pile lengths L
for i = 1:length(L);

    %..............................................................
    % Looping over frequencies f
    for ii=1:length(f_vector)
        f = f_vector(ii);
        omega = 2*pi*f;

        %..............................................................
        % Looping over wavenumbers xsi
```

```
        for ix=1:length(xsi_vector)
            xsi=xsi_vector(ix);

            %.............................................................
            % Coefficient matrices of elastic continuum
            alpha = sqrt(xsi^2 - omega^2/(c_1_damp^2));
            beta = sqrt(xsi^2 - omega^2/(c_2_damp^2));
            u_12 = n/r*besselk(n,alpha.*r) - alpha.*besselk(n+1,alpha.*r);
            u_14 = 1i*xsi.*besselk(n+1,beta*r);
            u_16 = n/r*besselk(n,beta.*r);
            u_22 = -n/r*besselk(n,alpha.*r);
            u_24 = u_14;
            u_26 = -n/r*besselk(n,beta.*r) + beta.*besselk(n+1,beta.*r);
            u_32 = 1i*xsi.*besselk(n,alpha.*r);
            u_34 = beta.*besselk(n,beta.*r);
            u_36 = 0;
            U = [u_12 u_14 u_16;u_22 u_24 u_26;u_32 u_34 u_36];
            t_12 = (2*mu*(n^2-n)/r^2-lambda*xsi.^2 + ...
                (lambda+2*mu)*alpha.^2).*besselk(n,alpha.*r) + ...
                    2*mu*(alpha./r).*besselk(n+1,alpha.*r);
            t_14 = -2*mu*1i*xsi.*beta.*besselk(n,beta.*r) - ...
                2*mu*1i*xsi.*(n+1)./r*besselk(n+1,beta.*r);
            t_16 = 2*mu*(n^2-n)/r^2.*besselk(n,beta.*r) - ...
                2*mu*n./r.*beta.*besselk(n+1,beta.*r);
            t_22 = -2*mu*(n^2-n)/r^2.*besselk(n,alpha.*r) + ...
                2*mu*n/r.*alpha.*besselk(n+1,alpha.*r);
            t_24 = -mu*1i*xsi.*beta.*besselk(n,beta.*r) - ...
                2*mu*1i*xsi*(n+1)./r.*besselk(n+1,beta.*r);
            t_26 = (-2*mu*(n^2-n)/r^2-mu*beta.^2).*besselk(n,beta.*r) ...
                - 2*mu*beta/r.*besselk(n+1,beta.*r);
            t_32 = 2*mu*1i*xsi*n/r.*besselk(n,alpha.*r) - ...
                2*mu*1i*xsi.*alpha.*besselk(n+1,alpha.*r);
            t_34 = mu*n/r*beta.*besselk(n,beta.*r) - ...
                mu*(xsi.^2+beta.^2).*besselk(n+1,beta.*r);
            t_36 = mu*1i*xsi*n/r.*besselk(n,beta*r);
            T = [t_12 t_14 t_16;t_22 t_24 t_26;t_32 t_34 t_36];
            K_z(ix) = -2*pi*a*[0 0 1]*T*(U\[0 0 1]');

            % ........................................................
            % (STEP 1) Calculating response of infinite pile
            U_z(ix) = f_0./(E_pile*A*xsi.^2 + K_z(ix) - ...
                m_prim*omega.^2); % eq.9
        end
        U_xsi_matrix(ii,:) = U_z; % displacement matrix (omega,xsi)

        % ...............................................................
        %(STEP 2) Transform the frequency response into space domain..
        u_z_matrix(ii,:) = fftshift(ifft(U_z)*xsi_max)/2/pi; % ...
            Displacement matrix (omega,z)
```

```
        u_0(ii)=u_z_matrix(ii,Nz/2+1); % Displacement at excitation ...
            point (z=0)
        %  ...and evaluating corresponding force P at z=L and z=-L
        [iz]=find(z≥L(i),1,'first');
        dudz = (u_z_matrix(ii,iz+1)-u_z_matrix(ii,iz-1)) / (2*dz); % ...
            Central difference
        P = E_pile*A*dudz;

        % ...........................................................
        % (STEP3) Applying mirror forces at z=L and z=-L on infinite ...
            pile in Fourier domain
        fL1 = -P.*exp(-1i*xsi_vector*L(i));
        fL2 = -P.*exp(1i*xsi_vector*L(i));
        % ..calculating response of forces in frequency domain..
        U_zL = (fL1 + fL2)./(E_pile*A*xsi_vector.^2 + K_z - ...
            m_prim*omega.^2); % eq.9
        % ..and transforming response to space domain
        u_zL_matrix(ii,:) = fftshift(ifft(U_zL)*xsi_max)/2/pi; % ...
            disp.-matrix (omega,z)

        % ...........................................................
        % (STEP 4) Superimposing displacement responses (Step 2 and ...
            3)to get
        % driving point respons for finite pile of length L.
        u_zL_super(ii,:) = u_z_matrix(ii,:) + u_zL_matrix(ii,:);
        u_0_super(ii)=u_zL_super(ii,Nz/2+1);
    end
u_L(i,:) = u_0_super;
end
toc
```